TAMPEREEN TEKNILLINEN YLIOPISTO
TAMPERE UNIVERSITY OF TECHNOLOGY

OLLI PEKKALIN

INDOOR DEAD RECKONING SYSTEM

Master of Science Thesis

Examiners: Prof. Jukka Vanhala
Prof. Jarmo Takala
Examiners and topic approved by the
Faculty Council of the Faculty of
Computing and Electrical Engineering
on 11 January 2012.

ABSTRACT

TAMPERE UNIVERSITY OF TECHNOLOGY
Master's Degree Programme in Signal Processing and Communications Engineering
OLLI PEKKALIN : Indoor Dead Reckoning System
Master of Science Thesis, 53 pages, 0 Appendix pages
December 2013
Major: Design of Electronic Circuits and Systems
Examiners: Prof. Jukka Vanhala and Prof. Jarmo Takala
Keywords: dead reckoning, positioning, gyroscope, odometer

In this thesis a positioning system, that can provide accurate reference coordinates for indoor usage is described and analysed. Those coordinates are needed in the development of various indoor positioning systems. Satellite navigation systems such as GPS can provide accurate positioning outdoors but their accuracy is poor when used indoors. Inertial navigation can provide accurate positioning indoors using accelerometers and gyroscopes but an accurate system is extremely expensive. Accurate indoor positioning is also achievable using a floor plan, a measuring tape or both but these methods are prone to human errors. The system presented in this thesis is designed to overcome the aforementioned problems using dead reckoning navigation. Dead reckoning is a positioning method, that starts always from a known location and attitude. In dead reckoning, gyroscope and odometer measurements are used to obtain position by updating the previous position.

The dead reckoning system uses a micro electro mechanical (MEMS) gyroscope and two odometers to measure attitude and travelled distance, respectively. A data acquisition program was written to save their measurements to log files on a PC and position was computed by post processing those. The system has been mounted on a cart for easy transportation.

Before testing accuracy of the system the gyro and odometers were calibrated. The gyro was attached to a turn table to calibrate its scale factor and bias. From the turn table study it became obvious that the gyro needs to be calibrated just before testing accuracy of the system. Odometers were calibrated by driving the cart in a known straight line distance several times. Based on the drives a scale factor was calculated to compensate the difference in odometer readings.

The gyro scale factor was calibrated just before accuracy test of the system by turning the cart around several times. The accuracy of the system was tested in a test drive lasting 30 minutes. During the test the gyro bias was calibrated whenever the system was stopped at reference positions for positioning accuracy estimation. Positioning error of less than 30 cm was achieved in the test drive.

TIIVISTELMÄ

TAMPEREEN TEKNILLINEN YLIOPISTO
Signaalinkäsittelyn ja tietoliikennetekniikan koulutusohjelma
OLLI PEKKALIN: Vektorisuunnistukseen perustuva sisätilapaikannusjärjestelmä
Diplomityö, 53 sivua, 0 liitesivua
Joulukuu 2013
Pääaine: Elektroniikan laitesuunnittelu
Tarkastajat: Prof. Jukka Vanhala ja Prof. Jarmo Takala
Avainsanat: vektorisuunnistus, paikannus, gyroskooppi, matkamittari

Tässä työssä kehitettiin ja analysoitiin tarkka sisätilapaikannusjärjestelmä. Sitä voidaan käyttää tarkkojen koordinaattien määrittämiseen, joita tarvitaan kehitettäessä muita sisätilapaikannusjärjestelmiä. Satelliittipaikannusjärjestelmiä, kuten GPS:ää, voidaan käyttää ulkotiloissa tarkkojen koordinaattien määrittämiseksi, mutta sisällä niiden tarkkuus on heikko. Tarkkaan sisätilapaikannukseen soveltuvat esimerkiksi gyroskooppeja ja kiihtyvyysantureita käyttävät inertiapaikannusjärjestelmät, mutta ne ovat erittäin kalliita. Pohjapiirustusta, mittanauhaa tai molempia voidaan käyttää tarkkaan sisätilapaikannukseen, mutta niitä käytettäessä tulee tehtyä helposti virheitä. Työssä esitetty vektorisuunnistusjärjestelmä on suunniteltu ratkaisuksi edellä mainittuihin ongelmiin. Vektorisuunnistus on paikannusmenetelmä, joka alkaa aina tunnetusta sijainnista ja suunnasta. Siinä käytetään gyroskoopin ja matkamittarin mittauksia paikan määrittämiseksi päivittämällä edellinen sijainti.

Työssä esitetty järjestelmä käyttää mikromekaanista (MEMS) gyroskooppia suunnan määrittämiseksi ja kahta matkamittaria kuljetun matkan mittaamiseksi. Mittausten lukemiseksi antureilta kirjoitettiin tietokoneohjelma, joka tallensi ne lokitiedostoihin. Järjestelmän sijainti määritettiin jälkikäteen käyttäen lokitiedostoihin tallennettuja mittauksia. Järjestelmä on kiinnitetty kärryyn, jotta sitä on helppo kuljettaa sisätiloissa.

Järjestelmän gyroskooppi ja matkamittarit kalibroitiin ennen sen tarkkuuden tutkimista. Skaalauskertoimen ja biaksen määrittämiseksi gyroskooppi kiinnitettiin pyörityspöytään. Kalibrointituloksista kävi ilmi, että gyroskooppi täytyy kalibroida juuri ennen järjestelmän tarkkuuden tutkimista. Matkamittarit kalibroitiin työntämällä kärryä suoraan tunnetun pituinen matka, jonka mittaus toistettiin useampia kertoja. Mittausten perusteella määritettiin skaalauskerroin, jolla kompensoitiin matkamittareiden lukemissa havaittu ero.

Gyroskoopin skaalauskerroin kalibroitiin juuri ennen järjestelmän tarkkuuden tutkimista pyörittämällä kärryä useampi kerta ympäri. Järjestelmän tarkkuutta tutkittiin koeajossa, joka kesti 30 minuuttia. Koeajon aikana gyroskoopin bias kalibroitiin aina pysähdyttäessä tunnetuissa sijainneissa paikannustarkkuuden tutkimiseksi. Paikannusvirhe koeajon aikana oli alle 30 cm.

PREFACE

The research presented in this thesis has been carried out at Tampere University of Technology, Department of Computer Systems. It has received funding from the European Union's Seventh Framework Programme (FP7/2007-2013) under grant agreement number 227890 (GRAMMAR project). Focus of this thesis was to develop an accurate indoor positioning system, that can used as a reference in the research of various indoor positioning systems.

This work was supervised by Professor Jarmo Takala and Professor Jukka Vanhala. I would like to thank both of them for examining my thesis and Jarmo also for giving me valuable support needed all the way during the research. I would like to thank especially M.Sc. Helena Leppäkoski for giving me advice and support. I'm also grateful for all the former colleagues at the department for their support.

Finally, I would like to thank my family and friends for their support and understanding.

Tampere, 15 October 2013

Olli Pekkalin

CONTENTS

LIST OF ABBREVIATIONS AND NOTATION

accelerometer	a device that measures acceleration
API	Application Programming Interface (a communication interface between software components)
ASCII	American Standard Code for Information Interchange (a way of representing text in digital devices)
Bluetooth	a radio communication technology for short distances
bus	a transmission line where several devices can communicate
CS	Chip Select (a signal of SPI)
dead reckoning	a positioning method where position estimate is obtained by updating the previous position using attitude and odometer measurements
dropout	difference between input and output voltage in a regulator
embedded system	a computer system with a dedicated function within a larger system
fingerprinting	a positioning method that exploits relationship of any measurable physical stimulus and a location
FOG	Fiber-Optic Gyro (a type of gyroscope)
full-duplex	communication where data can be sent and received simultaneously
gyro	gyroscope
gyroscope	a device that measures or maintains orientation
GNSS	Global Navigation Satellite System (a system of satellites that provides global positioning)
GPS	Global Positioning System (a GNSS)
half-duplex	communication where data can be sent and received but not simultaneously
HRG	Hemispherical Resonator Gyro (a type of gyroscope)
I2C	Inter-Integrated Circuit (a bus type)
IMU	Inertial Measurement Unit (a device containing typically three gyros and accelerometers, used for inertial navigation)
inertial navigation	a positioning method where position estimate is obtained by updating the previous position using gyro and accelerometer measurements
LDO	Low DropOut (small dropout of a regulator)
LED	Light Emitting Diode
linear regulator	a regulator that changes its resistance depending on load to maintain a constant voltage

map matching	process of aligning estimated user positions with a map
master device	a device that communicates and controls communication on a bus
MEMS	Micro Electro Mechanical Systems (a technology of very small electro mechanical systems)
MISO	Master In Slave Out (a signal of SPI)
modulation	process of varying properties of a periodical signal with a modulating signal that contains information
MOSI	Master Out Slave In (a signal of SPI)
multi-path effect	radio signals reach a receiver using several paths causing interference and phase shift in the signals
PDR	Pedestrian Dead Reckoning (dead reckoning navigation for pedestrians)
positioning cart	the dead reckoning system presented in this thesis mounted on a cart
ppm	parts per million
PWM	Pulse-Width Modulation (a modulation where pulse width varies)
real-time operating system	an operating system that reacts to a steady flow of information without interruption
regulator	a device that maintains constant voltage level
RLG	Ring Laser Gyro (a type of gyroscope)
RS-232	Recommended Standard 232 (a serial communication standard)
RS-422	Recommended Standard 422 (a serial communication standard)
RS-485	Recommended Standard 485 (a serial communication standard)
SCK	Serial ClocK (a signal of SPI)
SCL	Serial CLock (a signal of I2C)
SDA	Serial DAta (a signal of I2C)
serial transmission	transmission where data is send sequentially one bit at a time
slave device	a device that communicates on bus when given a permission by a master device
SPI	Serial Peripheral Interface (a bus type)
transceiver	a device that can transmit and receive
transmission line	a system of conductors that transfer electrical signals between locations
unwrap	allow a bounded number to go over or under its bounds
USB	Universal Serial Bus (a common bus in computers)
VBA	Vibrating Beam Accelerometer (a type of accelerometer)
WLAN	Wireless Local Area Network (a radio communication link between two or more devices)

Δt_k	length of sampling interval at sampling time k
Δs_k	travelled distance within a sample interval at sampling time k
ψ_k	heading at sampling time k
ω_k	angular rate at sampling time k
ω_k^g	measured angular rate at sampling time k
$\omega_x(t)$, $\omega_y(t)$, $\omega_z(t)$	angular rate of axis x, y and z
$\omega_x^g(t)$	gyroscope output angular rate of x axis
$a_x(t)$, $a_y(t)$, $a_z(t)$	acceleration of axis x, y and z
$a_x^a(t)$	accelerometer output acceleration of x axis
B	bias
$B(t)$	bias
$B_d(t)$	dynamic component of bias
B_s	static component of bias
E_0	initial east coordinate
E_k	east coordinate at sampling time k
g	acceleration due to gravity
$M_y(t)$, $M_z(t)$	cross-coupling coefficient of y and z axis
N_0	initial north coordinate
N_k	north coordinate at sampling time k
$n_x(t)$	random noise
S	scale factor
$S_x(t)$	scale factor of x axis
v	velocity
$v_x(t)$	velocity of x axis
$v_x^o(t)$	odometer output velocity of x axis
x_0	initial x coordinate
x_k	x coordinate at sampling time k
y_0	initial y coordinate
y_k	y coordinate at sampling time k

1. INTRODUCTION

Accurate reference positions are needed in the development of indoor positioning systems in order to assess their performance. Accuracy of the reference positions must be considerably higher than the systems they are compared with. Relatively accurate reference positions are also needed when setting up a positioning system based on fingerprinting to create a database containing mapping between them and measured physical stimuli. Fingerprinting systems can be based on any measurable physical stimulus that has a relationship with location. They can be based on for example WLAN (Wireless Local Area Network) or Bluetooth radio communication technologies [1, 2]. In fingerprinting the user's position is obtained by comparing a measured physical stimulus with the database created in set up phase of the system.

Global Navigation Satellite Systems (GNSS) such as Global Positioning System (GPS) can be used to provide accurate position estimates outdoors. Indoors a GNSS positioning receiver needs aiding in order to provide accurate position estimates. There the receiver has poor visibility to the satellites in the sky. The poor visibility together with signals reaching the receiver using several paths, causing interference and phase shifting (multipath effect), makes positioning inaccurate. Assisted GPS (A-GPS) uses aiding to improve positioning accuracy but due to the aforementioned effects, it is difficult to achieve accuracy better than 70 m indoors [3]. Therefore, neither GPS nor A-GPS is suitable technique for accurate indoor positioning.

An accurate position estimate can be obtained indoors by using an Inertial Measurement Unit (IMU). An IMU typically contains three gyroscopes (gyros) and three accelerometers. It does not require any external sources for navigation. Inertial navigation using an IMU requires only knowledge of the initial position, attitude and velocity. The gyros are used to update the attitude based on the previous attitude estimate and the accelerometers are used for updating the velocity. The position estimate is obtained by integrating the velocity measurements and adding those to the previous position estimate. [4]

In order to obtain an accurate long-term navigation solution, an IMU has to be extremely accurate. Such IMUs are available but they are very expensive. For example, an IMU of tactical grade that can be used for stand-alone inertial navigation for a few minutes costs from 5,000 to 20,000 USD [3]. After a minute its horizontal position error is approximately 5 m and after an hour the error has grown to 19 km [5]. Accurate stand-

alone inertial navigation for an hour can be obtained by using an marine grade IMU that costs about 1,000,000 USD [3]. Its navigation solution drifts typically less than 1.8 km per day [5]. IMUs are too expensive for many indoor navigation purposes. This applies also to their usage as reference positioning systems to assess performance of indoor navigation systems. An inexpensive solution for accurate indoor positioning is to use a floor plan, a measuring tape or both. These methods are time consuming and prone to human errors.

Due to shortcomings of the previously mentioned methods a positioning system, presented in this thesis, has been designed. It can automatically measure indoor reference positions. The system uses dead reckoning to obtain accurate position estimates.

Dead reckoning is a positioning method where the position is obtained by updating the previous position. An initial position and attitude must be known to use this positioning method. The position is updated based on measuring the travelled distance and its attitude. Changes of the coordinates are calculated using the travelled distance from the previous position and its attitude. The updated position is obtained by adding the coordinate changes to the previous position.

In this thesis, a positioning system based on dead reckoning is implemented and its performance is analysed. The system provides accurate position indoors that can be used as a reference for other indoor positioning systems. In this system, an accurate gyroscope is used for estimating attitude of the system and the travelled distance is obtained using two wheel encoders. The position of the system is obtained by post processing the data of the gyro and encoders that are saved to files using a PC. After calibration of the sensors the positioning error in a test drive lasting 30 minutes was less than 30 cm.

In the beginning of this thesis, introductions to dead reckoning and dead reckoning sensors (chapters two and three, respectively) are given. In chapter four, the system components are introduced. System software from data acquisition to position estimation is presented in chapter five. Calibration of the system, positioning test route and test results are presented in chapter six. In chapter seven, conclusions of this thesis are presented. Most of the results presented in this thesis have already been published in [6].

2. DEAD RECKONING

Dead reckoning is a positioning method, where a position estimate is obtained by updating the previous position [4]. An initial position is needed for the position update. The position update is based on measuring the travelled distance and its attitude. Heading can be used as an attitude measurement for two dimensional navigation, whereas three dimensional needs a three component attitude measurement. If an attitude measurement provides only change of attitude, then initial attitude must also be known. This chapter focuses on two dimensional navigation.

The concept of dead reckoning is shown in Figure 2.1. In the Figure the cross is the initial known position where dead reckoning computation begins. The dashed lines with arrows in the end illustrate the travelled distances and their attitudes between position estimates. The estimated positions are marked with black dots surrounded by circles. The circles represent the uncertainty of the estimates [4]. The uncertainty may also be elliptical instead of circle since distance and attitude measurements can have different accuracies. Each time a position is estimated by updating the previous position estimate, some errors are added to the calculation [4]. This leads to growing uncertainty of the position estimates [4].

2.1 Attitude Measurement

Attitude can be measured using several methods. One way to obtain attitude is to use angular rate measurements. To obtain attitude from angular rate measurements, an initial heading is needed. [4]

The heading can be estimated, without any initialisation, by using an accurate angular rate gyroscope. It is capable of detecting the Earth's rotation rate, from which the heading can be obtained. To measure the Earth's rotation the gyro has to be well calibrated. When the sensitive axis of a gyro points to the north or south the measured angular rate has the greatest magnitude. The sign of the measured angular rate distinguishes between the north and south. If the sensitive axis is pointing to the east or west, the measured angular rate is zero. During the measurement the gyro must be stationary, thus this method can not be used during movement. [7]

Angular rate measurements can be used to propagate heading when its initial value ψ_0 is known. One way to obtain the initial heading is to use the aforementioned Earth's rotation rate measurements. After the initial heading has been obtained, the heading can

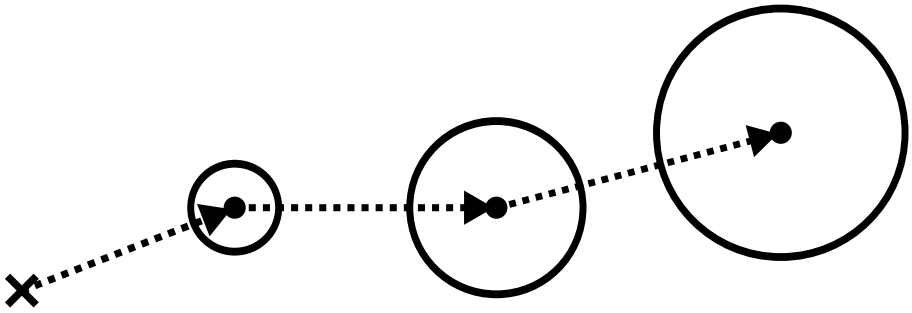

Figure 2.1. *Dead reckoning [4]*

be propagated by

$$\psi_k = \psi_{k-1} + \Delta t_k \left(S\omega_k^g + B \right) \tag{2.1}$$

where Δt_k is length of the sampling interval, S is the scale factor, ω_k^g is the measured angular rate, and B is the bias [8]. The propagation equation presented in 2.1 uses uncalibrated angular rate measurements from a sensor. The true angular rate ω_k can be obtained from the measured one using equation

$$\omega_k = S\omega_k^g + B. \tag{2.2}$$

It can be used to simplify the equation 2.1 to obtain the heading propagation equation

$$\psi_k = \psi_{k-1} + \Delta t_k \omega_k \tag{2.3}$$

where the true angular rate is used.

Flux density of the Earth's magnetic field depends on heading, hence heading can be obtained from a flux density measurement. The Earth's magnetic field points from the magnetic north pole to the magnetic south pole through the Earth, and takes the opposite path through the atmosphere. Thus it is horizontal at the equator and vertical at the poles. The magnetic north and south pole move slowly: in year 2005, the magnetic field was inclined about 10° to the Earth's rotation axis. Flux density of the field can be used to obtain the magnetic heading. It can be obtained using a mechanical compass that is sensitive to the magnetic field. A magnetometer can be used as an electronic compass. It measures the total magnetic flux density from which the magnetic heading can be obtained. Two or three orthogonally mounted magnetometers are used together to obtain the heading. The true heading can be obtained from the magnetic one by adding the declination of the Earth's magnetic field to it. [4]

2.2 Odometer Measurement

Odometers are used for measuring the velocity and travelled distance of a land vehicle. With two odometers, the heading changes can also be measured. Those are obtained by differentiating the measurements of two odometers. This technique is called differential odometry. [4]

Odometers typically measure rotation of the transmission shaft or wheel axle. Wheel diameter must be known to obtain the travelled distance from the rotation. By differentiating the distance measurements, velocity can also be obtained. [4]

2.3 Position Update

Dead reckoning method is based on position updates. The updates use attitude and odometer measurements to propagate position estimates. Instead of odometer measurements, the travelled distance, needed for position updates, can also be obtained using other techniques. In pedestrian dead reckoning, the travelled distance is obtained from steps during walking. This is explained in more detail in the following section.

To propagate position, the previous position must be available. Thus it requires that initial north and south coordinates N_0 and E_0 are known in order to use dead reckoning. Position is propagated by

$$\begin{aligned} N_k &= N_{k-1} + \Delta s_k \cdot \cos(\psi_k); \\ E_k &= E_{k-1} + \Delta s_k \cdot \sin(\psi_k) \end{aligned} \tag{2.4}$$

where N_k is the north coordinate, E_k is the east coordinate, Δs_k is the travelled distance within a sample interval and ψ_k is the heading [8].

Instead of north and east coordinates it sometimes is easier to use a local coordinate system. The coordinate system can be aligned with for example walls of a building for indoor navigation purposes. Based on equation set 2.4 the local coordinates are propagated by

$$\begin{aligned} x_k &= x_{k-1} + \Delta s_k \cdot \cos(\psi_k); \\ y_k &= y_{k-1} + \Delta s_k \cdot \sin(\psi_k) \end{aligned} \tag{2.5}$$

where x_k is the x coordinate of the local coordinate system and y_k the y coordinate of it. Initial coordinates x_0 and y_0 must also be known when a local coordinate system is in use.

On each update uncertainty of the position estimate grows. The uncertainty is caused by distance and attitude measurement errors. The accuracy of position estimates during attitude changes depend on the frequency of the position updates. It can be improved by more frequent updating. [4]

2.4 Pedestrian Dead Reckoning

Pedestrian navigation is a challenging task, because pedestrians can move in places where coverage of satellite navigation systems such as GPS is poor. Motion can be recognised using accelerometers and gyroscopes (described in chapter 3) but if their measurements are used directly for navigation the sensors should be very accurate. The problem with accurate accelerometers and gyros is that those are expensive and some of them have also a large size. Thus those are not suitable for pedestrian navigation, where the price should be low and size of the sensor small. The solution for pedestrian navigation is to use inexpensive and small gyros and accelerometers to count steps. In addition to travelled distance obtained from step counting, heading needs to be obtained to estimate position. Heading can be obtained using aforementioned techniques of attitude measurement. This navigation technique is called pedestrian dead reckoning (PDR). [4]

The PDR algorithm has three phases: step detection, step length estimation and position update. Step detection is used to identify that a step has been taken. Step length estimation is needed because the length varies not only between individuals but also for a single person. It changes depending on obstacles, slope and texture of terrain, tiredness of a person, and whether the person is walking alone or with others. At last the position is updated based on measured distance from the steps and obtained attitude. Either equation 2.4 or 2.5 is used for the update. [4]

Only accelerometers are typically used for step detection in PDR systems [4]. Single accelerometer can be mounted vertically on body or along the forward axis of a shoe. An accelerometer triad consisting of three orthogonally mounted accelerometers can also be used [9]. It enables step detection independent of pedestrian's orientation.

Steps can be easily recognised from the acceleration of foot mounted sensors. Their acceleration is constant when the foot is in ground and changing when it swings [4]. Vertical acceleration of body mounted sensors produce double peaked signal during walking [4]. Steps can be detected from acceleration zero crossings, when the specific force goes over or drops below the acceleration due to gravity (g) [4]. In addition to double peaks caused by walking, the signal can have also smaller peaks caused by measurement noise, unwanted movement of sensor about its mounting point, and irregular user movement [10]. Instead of zero crossings, steps can be detected from a sequence of local minimum and maximum values [10]. If a local minimum and maximum has occurred within a set time limit and difference between the values is greater than a set limit, a step has been taken. One way to detect steps is to use measurements of an accelerometer triad [9]. Root of sum of squares for accelerations measured with an accelerometer triad during walking can be seen in Figure 2.2. All of the high peaks in the figure, all together eight of them, are steps. Peak detection with an correctly set threshold can be used to detect steps from the signal shown in the figure.

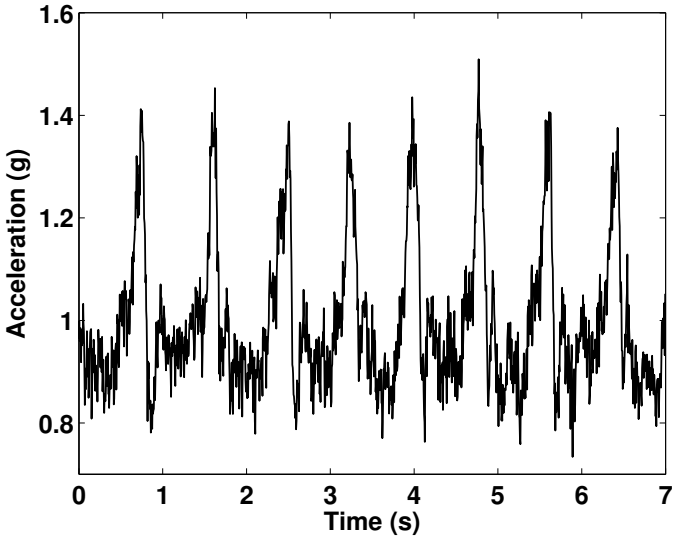

Figure 2.2. *Total acceleration during walking (root of sum of squares)*

PDR can be implemented using a fixed step length but the accuracy is worse than using an estimated length [4]. When a fixed step length is used the error in distance measurement is approximately 10 % of the travelled distance [11]. Step length has been found to approximately vary as a linear function of the step frequency [12]. It correlates also with the slope of terrain [13], vertical velocity and variance of acceleration [14]. Step length can be modelled as a linear combination of terms dependent on these parameters and a constant value [14, 15]. With the model 3 % error in the travelled distance can be achieved. Fixed step length and parameters for the model can be calibrated outdoors using GPS to provide reference distance [4].

3. DEAD RECKONING SENSORS

Dead reckoning navigation is based on measuring heading and travelled distance as mentioned earlier. An initial position is needed in order to use dead reckoning. If the heading is based on updating the previous value, then an initial heading is also needed. The heading can be updated using data from a gyroscope that measures either angle or angular rate. The travelled distance can be measured using an odometer. Instead of an odometer, a high quality accelerometer can be used to measure the travelled distance. The distance is obtained from the measured acceleration through integration.

3.1 Gyroscope

Gyroscopes are used to sense the angle of an object compared to a baseline (displacement gyroscopes) or the angular rate of turn about an axis (rate gyroscopes). Rate gyroscopes are more common in use. First developed gyroscopes have been mechanical, also known as conventional, ones using inertial properties of a spinning wheel or rotor (spinning mass). Nowadays gyroscopes come in different forms and many of those use other means than a spinning mass to measure either turned angle or angular rate. These sensors are not actually gyros in the sense that they do not rely on dynamic properties of rotating bodies. They are classified as unconventional sensors since they use different methods than conventional mechanical gyroscopes to detect rotation. Several sensors in this class are actually angular rate sensors but since they provide body rotation they are still commonly called as gyroscopes. [16]

3.1.1 Different Types

The main types of gyroscopes are spinning mass, optical and vibratory. Other gyro technologies including nuclear magnetic resonance, angular accelerometers, flueric sensors, and atom interferometry have also been researched [4]. The original form of gyroscope makes use of the inertial properties of a rotor or wheel turning at a high speed [16].

A high-speed spinning rotor preserves its direction even though the gimbals are rotated. This is an example of a mechanical displacement gyro. [16]

Optical gyroscopes are based on principle that light travels at constant speed in an inertial frame. The path length for light sent in both directions around a closed-loop waveguide made of mirrors or optical fiber is the same when it is not rotating. When a waveguide is rotated about an axis perpendicular to its plane the path of the light beam

travelling to same direction as rotation becomes longer from the perspective of an inertial frame. Respectively the path becomes shorter for the light beam travelling to the opposite direction. This phenomenon is known as Sagnac effect. Angular rate of the waveguide with respect to inertial space can be determined by measuring changes in path length. [4]

A ring laser gyro (RLG) is an optical gyroscope that consist of a closed-loop tube filled with helium-neon gas mixture, also known as a laser cavity. The tube has at least three corners, each of those having a reflective mirror. Atoms in the gas are excited using electric field that leads to formation of two light beams travelling to opposite directions inside the laser cavity. Angular rate about an axis perpendicular to the cavity can then be determined from the changes in frequencies of light beams caused by the Sagnac effect. The beam travelling to same direction as rotation faces an increase in wavelength and a decrease in frequency and the opposite happens for the other beam. [4]

Interferometric fiber-optic gyro, also known as fiber-optic gyro (FOG) uses a fiber-optic coil to measure angular rate. Two light beams going to different directions are fed to a coil. The light beams come from a broadband light source that is divided into two equal portions using beam splitters. A detector is used to measure interference between the two combined beams. When the coil is rotated about an axis perpendicular to its plane the Sagnac effect introduces a phase change between the light beams. Angular rate of the gyro can be derived from the phase change seen as interference in the detector. [4]

Vibratory gyroscopes contain an element that is driven to harmonic motion [4]. The element can be for example a tuning fork, string, beam, pair of beams, ring, hemisphere or cylinder [4]. When the element is rotated about an axis orthogonal to the motion, a Coriolis acceleration is induced [16]. Operation of a vibratory gyro is based on detecting the Coriolis acceleration from which angular rate of the gyro can then be solved [16].

Most vibratory gyroscopes are low-cost and low-performance devices [4]. Majority of vibratory gyros are manufactured using MEMS (Micro Electro Mechanical Systems) technology and with quartz that gives better performance than silicon [4]. Hemispherical resonator gyro (HRG) is an exception from other vibratory gyros. The HRG is a high performance gyro that is suitable for space applications [4]. Typical for all vibratory gyros is that they are low power devices, reliable and start-up rapidly [16]. Some vibratory gyros are also very rugged [16].

Majority of MEMS gyros on the market belong to rate-grade class. Gyros in the class are suitable for automotive, consumer and medical usage. Their prices are on the order of 10 USD. A few companies are manufacturing tactical-grade MEMS gyros. Gyros in the tactical-grade class are suitable for robotics and military usage. Inertial-grade gyros have the best performance of all classes. Those can be used for inertial navigation and space research. So far only bulky constructions of MEMS gyros in this class exist costing millions of dollars. MEMS gyros are developing all the time and in the future there will be more tactical-grade and ultimately also inertial-grade gyros on the market. [17]

3.1.2 Errors and Calibration

The typical errors of a gyroscope are bias, scale factor, cross-coupling and random noise errors. The output of a gyroscope can be modelled as

$$\omega_x^g(t) = (1 + S_x(t))\,\omega_x(t) + B(t) + M_y(t)\omega_y(t) + M_z(t)\omega_z(t) + n_x(t) \tag{3.1}$$

where $\omega_x(t)$ is the true angular rate about the sensitive axis, $S_x(t)$ is the scale factor error, $B(t)$ is the bias, $M_y(t)$ and $M_z(t)$ are cross-coupling coefficients, $\omega_y(t)$ and $\omega_z(t)$ are angular rates about other axes, and $n_x(t)$ is the random noise. All error sources have four components: a fixed contribution, a run-to-run variation, a temperature dependent variation and an in-run variation. Each time the gyro is used the fixed contribution is present. It can be corrected by calibration of the gyro. The run-to-run variation is different each time the gyro is started but it remains constant within any run. It can not be corrected using laboratory calibration. The run-to-run variation can be corrected by integration with other sensors. The temperature dependent variation is correctable using laboratory calibration. The contribution of the in-run variation changes slowly during the course of a run. It can not be corrected using calibration but in theory it is correctable through integration with other sensors. [4, 16]

The bias error of a gyroscope is constant and exists in every sensor. It is independent of the angular rate and gravity. The bias can be modelled as

$$B(t) = B_s + B_d(t) \tag{3.2}$$

where B_s is static component and $B_d(t)$ dynamic component. The static component comprises run-to-run variation of the bias and residual fixed bias remaining after calibration. It is constant during operating period, but varies from run to run. The dynamic component is also known as in-run variation or instability of bias and it varies over periods of order a minute. It incorporates also the residual temperature-dependent bias, that has been left after calibration. It is typically about 10 percent of the static bias. [4]

To calibrate the bias of a rate gyroscope the gyro must be held stationary for a while. When the gyro is stationary its output is averaged and the bias is the result. The average incorporates other error sources such as cross-coupling errors and earth rotation rate but those are normally negligible compared to the gyro bias. The calculated bias is the long term fixed bias and with this calibration the aforementioned bias errors are left in the gyro output. [18, 19]

The scale factor error is the departure of the input-output gradient from unity. It is proportional to the true angular rate about the sensitive axis of the gyro. Illustration of the scale factor error can be seen in Figure 3.1. Increase in the true angular rate (input) causes the error in the output of a gyro to grow as can be seen in the figure. [4]

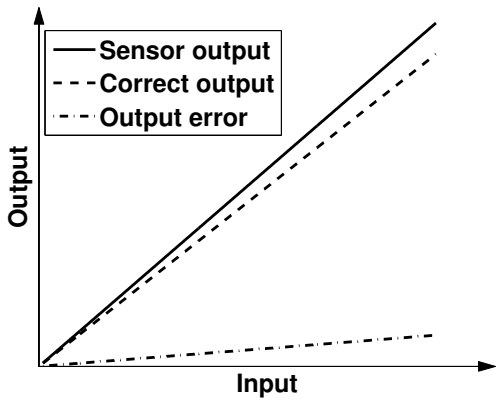

Figure 3.1. *Scale factor error [20, as cited in 4]*

Scale factor calibration of a rate gyroscope needs a known angular rate as reference. For accurate gyroscopes earth rotation rate can be used as a reference. Earth rotation rate is too small to be measured with cheap, low accuracy sensors, hence other reference is needed. A rotation table, that rotates with known angular rate, can be used as a reference. The scale factor can be calculated by taking off the bias from the gyro output during rotation and dividing the result by the reference angular rate. This calculation leaves still cross-coupling errors in the scale factor but it still provides quite good estimate of it. [19]

Cross-coupling errors arise from misalignment of the sensitive axes of a gyroscope with respect to the axes of the body frame due to limitations in manufacturing. These errors make gyros sensitive to orthogonal angular rate about its sensitive axis. The misalignment also produces scale factor errors, but those are typically two to four orders of magnitude smaller than the cross-coupling errors. In vibratory gyros the source of cross-coupling errors can be cross-talk between the individual sensors. [4]

The scale factor and cross-coupling errors are typically between 100 and 1,000 ppm (parts per million). MEMS gyros are an exception, for those these errors can be as high as 1 %. Ring laser gyros have typically low scale factor errors ranging from 10 to 100 ppm. Low cost gyros can have significant asymmetry in the scale factor, that leads to different errors for positive and negative angular rates. [4]

Random noise errors arise from numerous sources. The resolution of a sensor is limited by electrical noise, particularly in MEMS sensors, where signals are weak. In spinning mass gyros, mechanical instabilities exhibit noise. High frequency errors are exhibited in vibratory gyros. The high frequency errors average out over the order of a second when the gyro is not moving. However, if the gyro is rotating the noise will not be averaged out to same extent in navigation computation. Consequently, when selecting a gyro for highly dynamic applications caution should be exercised. A vibrating environment can also cause problems: if frequency of external vibration is close to resonating frequency of the gyro, there will be time correlated errors. [4]

Spinning mass and vibratory gyros are sensitive to accelerations along their axes due to mass unbalance. The sensitivity is called g-dependent bias. It is typically in the order of $1\ ^\circ/(\mathrm{h}\cdot\mathrm{g})$ but for uncompensated rate-grade class MEMS gyros it can be as high as $100\ ^\circ/(\mathrm{h}\cdot\mathrm{g})$. Every axis of a gyro can be sensitive to acceleration. [4]

3.1.3 Interfaces

There are gyroscopes on market with analog and digital interfaces. Analog rate gyroscopes produce output voltage that is proportional to the sensed angular rate. Digital rate gyroscopes incorporate analog to digital conversion inside the gyro and their output is a number proportional to the angular rate.

An example of an analog rate gyro is the LPR410AL [21] manufactured by STMicroelectronics. The typical output voltage of the gyro is 1.5 V when it is stationary. Counterclockwise rotation of the gyro increases the output voltage and clockwise rotation decreases it. The output voltage can then be converted to $^\circ/\mathrm{s}$ by taking off the stationary voltage, also known as bias, and dividing the result by its scale factor. The typical scale factor for the gyro is $10\ \mathrm{mV}/(^\circ/\mathrm{s})$ when measurement range is set to $\pm 100\ ^\circ/\mathrm{s}$.

Gyroscopes use numerous different digital interfaces. Some common digital interfaces for gyroscopes are SPI (Serial Peripheral Interface), I2C (Inter-Integrated Circuit), RS-232 (Recommended Standard 232), RS-422 (Recommended Standard 422) and RS-485 (Recommended Standard 485) [22, 23, 24]. The aforementioned interfaces use serial transmission, which means that the data is transmitted sequentially one bit at a time. Comparison of the interfaces can be seen in Table 3.1.

As seen from Table 3.1: SPI, I2C and RS-232 use single-ended signalling, where as RS-422 and RS-485 use differential signalling. Single-ended signalling uses a single conductor to carry a signal with respect to a reference voltage, usually ground. Differential signalling, in comparison, uses two conductors to carry a signal. In differential signalling the signal is difference between the conductors. An advantage of the differential signalling is that common errors added to the conductors during transmission are eliminated when the signal is formed using subtraction. The differential signal can be modelled as

$$V_{diff} = (V_+ + V_{error}) - (V_- + V_{error}) = V_+ - V_- \tag{3.3}$$

where V_+ is the positive part of the signal, V_- is the negative part, and V_{error} is the common error added on conductors used for the transmission, a system also known as a transmission line. In addition to two conductors, differential signalling also needs a reference voltage. Ground is usually used as the reference voltage. Change in the reference voltage is a common problem on long transmission lines. Differential signalling reduces the effect of the reference voltage change on the signal thus being more suitable for long transmissions than single-ended signalling. The suitability of differential signalling for

Table 3.1. *Comparison of digital interfaces [26, 27, 28, 29]*

	SPI	**I2C**	**RS-232**	**RS-422**	**RS-485**
Signaling	Single-ended	Single-ended	Single-ended	Differential	Differential
Maximum distance	< 3 m	< 3 m	15 m	1200 m	1200 m
Synchronisation	Sync.	Sync.	Async.	Async.	Async.
Duplex	Full	Half	Full	Half	Half
Maximum number of devices	multiple	multiple	2	1+10	32
Maximum data rate	> 1 Mbit/s	400 kbit/s – 3.4 Mbit/s	160 kbit/s – 1 Mbit/s	10 Mbit/s	10 Mbit/s
Minimal signal count (without needed ground)	3 + number of slaves	2	2	1	1

long transmissions can also be seen from Table 3.1: the differential RS-422 and RS-485 interfaces can be used for much longer transmissions than the single-ended SPI, I2C and RS-232. As differential interfaces RS-422 and RS-485 are also capable of higher data rates than single-ended SPI, I2C and RS-232. [25]

SPI and I2C buses (transmission lines where several devices can communicate) usually consist of a master device and one or several slave devices. The master device communicates and controls the communication on the bus and gives permission for a slave to communicate. Both SPI and I2C interfaces support multiple master devices, but most systems use only a master device. The number of devices on the bus is limited by bus capacitance and used data rate. Communication on both interfaces is synchronous, meaning that timing of data transmission uses a serial clock signal (called SCK in SPI and SCL in I2C). The clock signal is generated by the master device. [27, 28, 29]

In an SPI bus every slave has its own chip select (CS) signal. The master uses CS signals to control which slave device is active during a transmission. Before transmission starts the master selects a slave device using a CS signal. Master out slave in (MOSI) signal is used for transmitting data from a master to slave. Master in slave out (MISO) signal carries data from a slave device back to master. Data is transmitted from a master to slave and back simultaneously using MOSI and MISO signals. This simultaneous both ways communication is called full-duplex. [27, 28]

Every slave device has a unique address in I2C bus. The master device selects a slave device for transmission using its address. Data is transmitted both ways using a single SDA (serial data) signal, hence master can only send or receive data at a time. This kind of communication where a device can send and receive data but not at the same time is called half-duplex. When a transmission starts, the master sends a slave address with a bit indicating whether it will transmit or receive data with the slave device. After the slave has been selected communication follows on selected direction. [29]

As seen from Table 3.1: RS-232, RS-422, and RS-485 use asynchronous communica-

tion. In asynchronous communication there is no clock signal. Both the transmitter and the receiver have their own clock, which must be set to the same speed. When a transmission starts, the transmitter sends a start bit that is used to synchronise receivers clock for receiving the data that follows. When the data has been transmitted, the transmission ends after a stop bit or several stop bits. [30, 31]

RS-232 is a common serial interface found, for example, in many personal computers. It has been designed as an interface between two peripherals. Minimal signals needed for an RS-232 interface are receive and transmit. Data transmission can be controlled using control signals, which can be used, for example, for flow control. Using the flow control the receiver can inform that it is not able to receive data at the moment and the transmitter is not allowed to transmit. [27, 30, 31, 32]

RS-422 is a unidirectional serial interface. In RS-422 one transmitter device can send data to several receivers. It can have one transmitting and up to ten receiving devices. If the devices receiving the data need to communicate back to the transmitter, a separate bus is needed between receivers and the transmitter. If the separate return bus is added, the RS-422 interface is capable of full-duplex communication. [26, 27]

RS-485 interface uses a bidirectional bus for communication between several transceivers. A transceiver is a device capable of transmitting and receiving. RS-485 can have up to 32 transceiver devices, but there can be only one transmission at a time, hence it is capable of half-duplex communication. RS-485 interfaces that use two unidirectional buses are also available. If two unidirectional buses are used, the interface is capable of full-duplex communication. [27, 33]

3.2 Accelerometer

An accelerometer is used for measuring acceleration of an object. Operation of an accelerometer relies on Newton's laws. The laws tell that motion of an object will continue uniformly unless disturbed by an external force acting on the object. The laws also tell that the force will produce a proportional acceleration of the object. [16]

Acceleration measurement can be integrated to produce estimates of changes in velocity and position. An advantage of measuring changes in velocity and position using an accelerometer is that it can be done internally. If velocity and position changes are measured directly an external reference, such as ground, is needed. [16]

3.2.1 Different Types

Majority of accelerometers use either a pendulous or vibrating beam structure. Both technologies are based on the same principle for measuring acceleration. Pendulous designs have been used for decades, while first vibrating beam accelerometers have been manufactured in 1980s. Accelerometer designs can be divided into open-loop and closed-loop

categories. In open-loop designs proof masses are displaced and their movement is measured, where as in closed-loop systems proof masses are maintained in a fixed position and the force needed for maintaining the position is measured. [4, 34]

Basic construction of an open-loop pendulous accelerometer uses a proof mass attached to a case using an arm with hinge forming an pendulum. The pendulous arm enables the proof mass to move along its sensitive axis and prevents the movement in other directions. A spring or a pair of springs is connected to the arm to transmit force from the case to the pendulum. The hinge of the pendulum provides damping of movement. Acceleration is measured using a pickoff connected to the proof mass. The pickoff is typically a variable resistor. [4]

The open-loop pendulous accelerometer is a practical accelerometer but its performance is poor. It is limited by three factors. First, the pickoff is typically a variable resistor with bad resolution. Second, a spring exerts only approximately linear force when compressed or extended. The force exerted by a spring has non-linearity and hysteresis. Finally, the sensitive axis is perpendicular to the pendulous arm and it moves as the arm is moving with respect to the case. Result of the moving sensitive axis is non-linear response to acceleration about the desired sensitive axis and sensitivity to orthogonal acceleration. [4]

Precision pendulous accelerometers use closed-loop force-feedback designs to overcome these problems. In a force-feedback accelerometers the spring system of the open-loop design has been replaced with a torquer. The torquer maintains the pendulous arm at a constant position with respect to the case regardless of acceleration, thus the direction of the sensitive axis is also constant. The pickoff is used to detect movements from the equilibrium position and by adjusting torquer the pendulum is returned back to the constant position. In a force-feedback accelerometer the applied specific force is proportional to the force exerted by the torquer rather than the pickoff. The torquer can be made out of a pair of permanent magnets of opposite polarity mounted on both sides of the case and an electromagnet mounted on the pendulum. The pickoff can be capacitive, inductive or optical. [4]

The vibrating beam accelerometer (VBA) has a pendulous arm and proof mass similar to the pendulous accelerometer. In the VBA, the proof mass is supported along the sensitive axis by a vibrating beam. The movement of the arm is constrained by the beam with respect to the case. When a specific force is applied to the case along the sensitive axis, the proof mass is pushed or pulled by the beam causing the beam either to stretch or compress. The beam is vibrating at its resonant frequency driven by accelerometer electronics. Compression of the beam decreases its resonant frequency whereas stretching causes it to increase. Hence, the specific force along the sensitive axis can be obtained by measuring the resonant frequency of the beam. [4]

3.2.2 Errors and Calibration

As with gyroscopes, the typical error factors for accelerometers are bias, scale factor, random noise and cross-coupling. An accelerometer measurement can be modelled as

$$a_x^a(t) = (1 + S_x(t))\, a_x(t) + B(t) + M_y(t) a_y(t) + M_z(t) a_z(t) + n_x(t), \tag{3.4}$$

where $a_x(t)$ is the true acceleration along the sensitive axis, $S_x(t)$ is the scale factor error, $B(t)$ is the bias, $M_y(t)$ and $M_z(t)$ are cross-coupling coefficients, $a_y(t)$ and $a_z(t)$ are accelerations along other axes, and $n_x(t)$ is the random noise. As already explained for gyroscopes, all the errors have a fixed contribution, a run-to-run variation, an in-run variation and a temperature dependent variation. The fixed error contributions can be compensated with laboratory calibration whereas run-to-run variation changes between each run. The run-to-run variations may be correctable with the help of other sensors but it is not easy. The in-run variations change slowly during runtime and those can not be compensated using laboratory calibration. In theory the in-run variations are correctable by the integration with other sensors. The temperature dependent variations can be compensated using a laboratory calibration. [4, 16]

The bias is a constant error that exists in every accelerometer. It has been modelled in equation 3.2 for gyroscopes and the model is the same for accelerometers. It consist of a static and dynamic part. The static part is the same during an operation period but changes from run to run [4]. The dynamic part varies over periods of order a minute [4]. It also incorporates the temperature dependent bias left after calibration [4].

The scale factor error of an accelerometer is the departure of the input-output gradient from unity. In output of the accelerometer, it is seen as an error that is proportional to the true acceleration (input of the accelerometer) along the sensitive axis. The scale factor error has been presented in Figure 3.1. [4]

The bias and the scale factor of an accelerometer can be calibrated with the help of gravitation. Equation 3.4 is used for the calibration. The accelerometer is kept in two different known angles with respect to gravity, thus obtaining two equations with two unknown values, the scale factor $S_x(t)$ and the bias $B(t)$. Errors from other sources in the accelerometer output must either be calibrated beforehand or assumed to be zero in the equations to solve the scale factor and bias. [19]

Random noise errors arise from a number of sources. Particularly in MEMS sensors, where the signal is very weak, the resolution is limited by electrical noise. In pendulous accelerometers, mechanical instabilities cause noise. VBAs can exhibit high frequency resonances. When the accelerometer is stationary, high frequency errors average out in position calculation over the order of a second. If the accelerometer is moving the noise will not average out in calculation to the same extent. Care must be taken when selecting accelerometers for highly dynamic applications and vibrating environments. In vibrating

environments time correlated errors will arise if internal resonant frequencies are close to frequency of the vibration. [4]

Cross coupling errors arise from the misalignment of the sensitive axis with respect to the orthogonal axis of the body frame. The misalignment is caused by manufacturing limitations. This makes accelerometers sensitive to acceleration along the axes orthogonal to its sensitive axis. It also produces additional scale factor errors but those are typically two to four orders of magnitude smaller than the cross coupling errors. [4]

3.2.3 Interfaces

Like gyroscopes, accelerometers are also available with analog and digital interfaces. Analog interface accelerometers output a voltage that is proportional to the acceleration along the sensitive axis. Accelerometers with digital interfaces have internal analog to digital conversion and the output is a number proportional to the sensed acceleration.

An example of analog accelerometers is LIS332AR [35] manufactured by STMicroelectronics. It can measure three dimensional accelerations up to ± 2 g. In this model the scale factor is dependent on the supply voltage of the sensor (V_{dd}) being typically $0,2 \cdot V_{dd}$ V$/g$.

Accelerometers are on market with numerous digital interfaces. Common digital interfaces for accelerometers are SPI, I2C and RS-485 [36, 37]. Those interfaces have been described in section 3.1.3.

3.3 Odometer

Odometers measure travelled distance and the velocity of an object, typically a land vehicle. They usually measure rotation of the wheels. Some odometers use the Doppler effect of radio waves to measure the travelled distance and velocity. Those are attached to the moving object and they send radio waves to the surface underneath. The waves reflect back from the surface and by measuring their Doppler shift travelling velocity can be obtained. The velocity can then be integrated to calculate the travelled distance. [4]

3.3.1 Different Types

Odometers used in land vehicles typically use non-contact encoders to avoid mechanical wear. A toothed ferrous wheel is mounted on the transmission shaft or wheel axle. Magnetic flux density varies as teeth pass through a sensor. A sensor detects the variation and forms a signal from which travelled distance can be obtained. Cheap odometers use passive sensors based on variable reluctance. They are vulnerable to vibration and interference. They do not work at speeds below about 1 m$/$s and hence those are not recommended for navigation purposes. More expensive active odometers, often based on

Hall effect, work at all speeds. Optical odometers can also be used but those are vulnerable to dirt. [4]

Doppler radar measures travelling velocity directly from the surface underneath the moving object it is mounted to [4]. The radar sends radio waves and those reflect back from the surface [4]. Frequency shift of the reflected waves is then measured in the radar [4]. The frequency of the reflected waves change depending on velocity, this is known as Doppler effect. The Doppler shift frequency Δf of radar depends on velocity as follows

$$\Delta f = 2\frac{v f_0}{c}\cos(\theta) \tag{3.5}$$

where v is velocity of the object, f_0 is frequency of radar transmission, c is the speed of light and θ is the inclination angle of radio waves coming from the radar [38]. If the object is travelling away from the point where radio waves reflect from the ground, the frequency shift is negative and when moving towards the reflection point the shift is positive.

An example of a Doppler radar is the DICKEY-john Radar III [39] that can be seen in Figure 3.2. It is able to detect speeds from 0.5 km/h to 107 km/h. The radar gives out speed information without direction. Doppler radars with direction sensing are not commonly in use and are expensive, but studies about those have been carried out as in [40].

In some cases, it is necessary to be able to distinguish forward and backward movement. Odometers are typically only capable of producing a pulsed signal proportional to the travelled distance as mentioned. The travelling direction can not be detected from this signal, since same kind of pulses are produced on forward and backward movement.

Quadrature incremental encoders can be used as odometers that distinguish forward and backward movement. They can be produced using a disc with two code tracks. The tracks have 90° phase difference in sectors. Code tracks are lighted with an LED (Light Emitting Diode) from one side of the disc and signals from both tracks are obtained using

Figure 3.2. *Doppler radar*

detectors on the other side. The signals are called A and B. The phase difference in sectors results in the same phase difference in signals that can be used to obtain the travelling direction. [41]

3.3.2 Errors and Calibration

Typical measurement inaccuracies for wheel odometers are changes in wheel diameter, wheel slipping, skidding, and uneven road surface [42, 43]. The last three depend on terrain and their occurrence is unknown. This makes it hard to compensate their effect on travelled distance and velocity. A non-contact sensor such as a Doppler radar does not have these inaccuracies. It is robust and wheel slipping does not affect its output. [38]

Odometer velocity measurement can be modelled as

$$v_x^o(t) = (1 + S_x(t))\, v_x(t) + n_x(t), \tag{3.6}$$

where $S_x(t)$ is the scale factor, $v_x(t)$ is the true velocity and $n_x(t)$ is the random noise. The error in the velocity measurement caused by the scale factor depends linearly of the travelling velocity. The scale factor error has been presented in Figure 3.1. [38]

The calibration of an odometer needs a velocity or distance reference. When an odometer is used outdoors, satellite navigation systems can be used to provide a reference velocity measurement for the scale factor calibration [38]. If the calibration is done on road, a technique called map matching can be used to improve the accuracy of the satellite navigation system used as a reference [44]. In map matching a map is used to aid positioning in cases where it is known that the estimated position can not be anywhere on a map. For example if it is known that a car can only drive on road, then a position estimate being outside of a road is known to be erroneous. The erroneous position estimate can be corrected to be on the nearest road, thus improving accuracy of the position. When the satellite positioning accuracy improves, so does the reference velocity it provides for the calibration, thus improving accuracy of the calibrated odometer.

3.3.3 Interfaces

Land vehicle odometers typically output a pulsed signal. A pulse in the signal is proportional to the travelled distance. To obtain speed the signal is differentiated. [4]

Quadrature incremental encoders output two pulsed signals, A and B as described in Different Types section. A pulse in signal is proportional to the travelled distance. Travel direction can be obtained from the order of arrived pulses. If a pulse in signal A leads the vehicle is moving forward and if B leads it is moving backward. Travel direction can be also opposite for pulse arrival order, as this depends on installation of the wheel encoder. [41]

Doppler radars are on market with different interfaces. E.g., DICKEY-john Radar III comes with a pulsed signal output [39]. Frequency of the output signal is proportional to the travelling speed, being typically 27.3 $\mathrm{Hz}/\left(\mathrm{km}/\mathrm{h}\right)$. GSS series Doppler radars manufactured by Pegasem offer several interfaces [45]. Those come with a pulsed distance output, analog voltage speed interface and an RS-232 serial interface. With an additional interface box the GSS series radars offer speed pulse outputs and a USB (Universal Serial Bus) interface.

4. SYSTEM ORGANISATION

Accurate reference coordinates are needed for accuracy evaluation and set-up of indoor positioning systems. Those can be obtained, for example, by using a floor plan and measurement tape but that takes a lot of time and is prone to errors. The dead reckoning system was developed to overcome those challenges. In order to be usable, the system has to provide accurate positioning. The positioning error can be at maximum 1 m whenever the system is used, otherwise it can not be used to set-up or evaluate accuracy of indoor positioning systems. The system has to be also easy to move around and have possibility to transport other measurement devices. It must be battery powered to be able to move around.

The developed dead reckoning system consist of sensors, data acquisition devices, a computer and a cart. The computer collects all the data and runs the whole system. The cart is used for transporting the system and it can be also used to transport other measurement devices. The system with all the devices is also known as the positioning cart in this thesis.

4.1 System Description

The system contains an MEMS gyroscope (gyro) to estimate the heading of the cart and two wheel encoders to measure the travelled distance. A counter is used for counting the steps of the encoders. Angular rate data from the gyro and steps from the counter are transferred to the PC using USB (Universal Serial Bus), as shown in Figure 4.1.

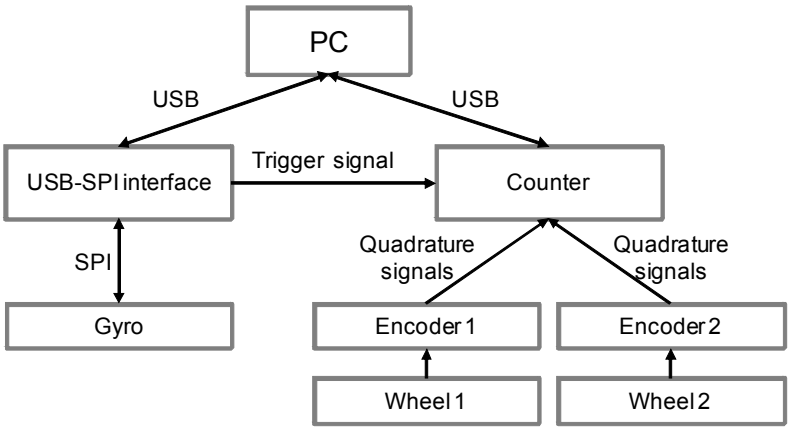

Figure 4.1. *System components*

The interface of the gyro is SPI. The USB-SPI interface is needed for acquiring data from the gyro to the PC. Measurement wheels are attached to axes of the encoders to measure the travelled distance. The encoders output quadrature signals to indicate steps from both forward and backward movement. The quadrature signals are connected to the counter, that counts steps of the encoders. A trigger signal from the USB-SPI interface is used for synchronizing data from the gyro and the counter.

The system can be seen in Figure 4.2. The gyro is inside the black case in front of the picture. It is attached to the plywood board of the cart using a clamp to keep it firmly in its place. On top of the cart is also the USB-SPI interface, the counter for the encoders, batteries, a power supply and the PC.

The distance measurement system, apart from the counter, has been mounted under the plywood board, as can be seen in Figure 4.3. The measurement wheels are mounted to the cart using spring arms in order to maintain good contact to floor despite of possible unevenness of the surface. The cart has fixed wheels at the back and turning wheels at the front. In order to prevent the measurement wheels from slipping sideways the wheels are installed at the back of the cart between the fixed wheels.

4.2 Components

The components shown in Figure 4.1 are the main parts of the system. In addition to the parts shown in the figure, the system also needs some additional parts to operate. In this section, a description is given for every component in the system.

4.2.1 Computer

A laptop PC powered by its own battery is used for collecting data from the sensors. The operating system of the computer is Windows XP. The USB-SPI interface and the counter for the encoders are connected to the computer using USB for data acquisition from the sensors. The computer runs a data acquisition program that saves data from the sensors to files. Dead reckoning computation is done after data acquisition using the saved data.

4.2.2 Gyroscope

To minimise errors in attitude measurement an accurate MEMS sensor was selected. The sensor is a prototype version of SCC1300-D02 [46], manufactured by VTI Technologies. The gyro is accurate enough to detect and estimate the Earth's rotation rate if factors affecting the bias are minimised and properly modelled [7]. In addition to the gyroscope, the sensors also include a three-axis accelerometer, which is not used for the results presented in this thesis. There are also two temperature sensors inside the SCC1300-D02, one for the gyroscope and the other for the accelerometer.

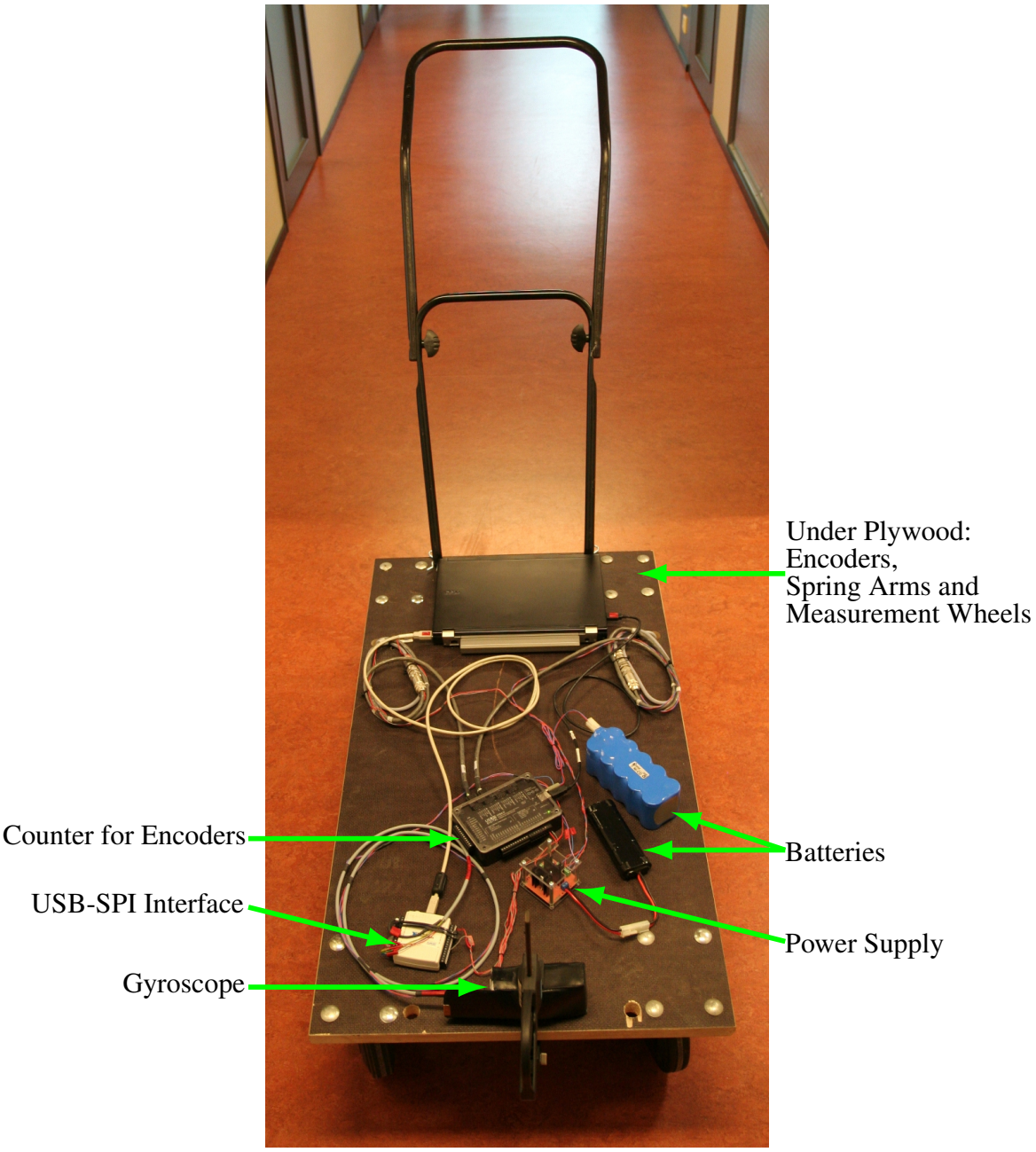

Figure 4.2. *Positioning cart*

The gyroscope can measure angular rates from $-100\ ^\circ/\text{s}$ to $100\ ^\circ/\text{s}$. Its bias stability is less than $1\ ^\circ/\text{h}$. Total scale factor error of the gyro is $\pm 2\ \%$ and its nonlinearity is $\pm 0.5\ \%$. The internal angular rate measurement frequency is $2,000$ Hz. [46, 47]

The gyro has a digital SPI interface. It uses 16-bit transfers and is capable of using clock frequencies from 100 kHz to 8 MHz. The latest angular rate measurement is stored in a 14-bit two's complement format in an internal register. It can be read from the register using the SPI interface. [46]

The gyroscope uses two different supply voltages. Analogue parts of the gyroscope need 5.0 V supply voltage whereas digital parts use 3.3 V. Analogue supply current of

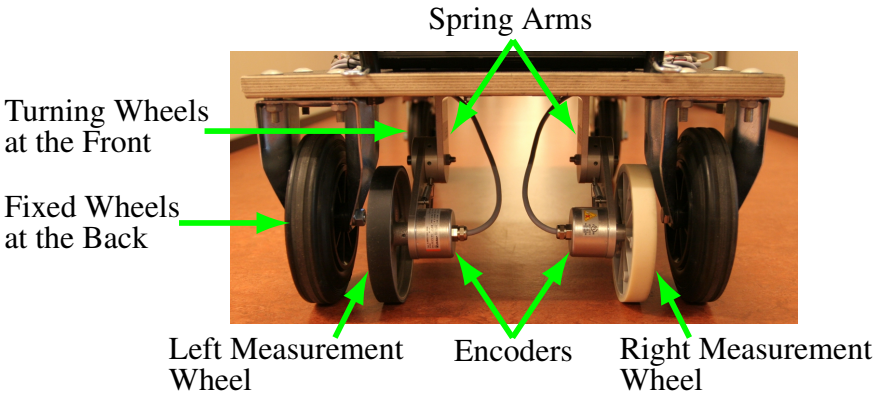

Figure 4.3. *Underneath the positioning cart from the back*

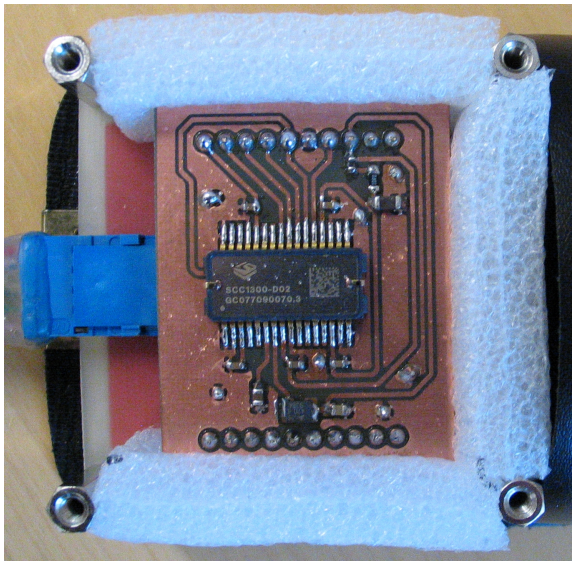

Figure 4.4. *The gyroscope and the insulation*

the gyroscope is typically 26 mA and digital is 20 mA. Even though the accelerometer is not used in this thesis, it is still powered on whenever the sensor has power. It uses a 3.3 V supply voltage for both analogue and digital parts. Current consumption of the accelerometer is typically 3 mA. [46]

The gyroscope can be seen in Figure 4.4. It has been soldered to the circuit board together with the external components suggested in [46]. The gyro has been insulated (white material around the circuit board) to prevent temperature changes in the sensor, that would produce errors in angular rate output. A cable is used to connect the gyro to the USB-SPI interface. Its blue connector can be seen on left side of the figure.

4.2.3 USB-SPI Interface

In order to connect the gyro to the PC an USB-SPI interface is needed. The National Instruments USB-8451 SPI/I2C interface was selected for this purpose. It connects to the computer using USB. The gyro communicates with the interface using SPI. The device

has, in addition to the SPI and I2C buses, also eight digital signals that can be used either as inputs or outputs. [48]

The interface can be controlled using a LabVIEW or C API (Application Programming Interface) provided with it [48]. In this thesis, the C API is used for controlling the interface. In addition to communicating with the gyroscope, a digital output signal of the interface is used for the synchronisation of the counter for the encoders.

4.2.4 Encoders

Odometer measurements are needed for dead reckoning in the system. Two encoders are used together with spring arms and measurement wheels to form two odometers. Detection of both forward and backward movement is needed in the system. Quadrature incremental encoders capable of distinguishing the direction of movement were selected to be used in the odometers.

The selected encoder model 8.5802.1241.2500 [49] is manufactured by Kübler. It has 2,500 steps per revolution of its 10 mm shaft. This model uses 5.0 V supply voltage and its typical current consumption is 40 mA. It has a quadrature output interface. The interface consists of signals A and B, from which both forward and backward steps can be detected. There is also a 0 output signal that indicates full revolutions. The 0 signal is not used in this system. All output signals are differential. A differential encoder model was selected to minimise errors in signals caused by noise. Operation of differential signalling has been presented in section 3.1.3 and a differential signal is modelled in equation 3.3.

4.2.5 Measurement Wheels

The measurement wheels are mounted to the encoders for measuring the travelled distance of the cart. Two different models (8.0000.3542.0010 and 8.0000.3552.0010) manufactured by Kübler were selected. The reason for selecting two different models was to see which one is better suited for distance measurement on floor. Floors can have different surfaces e.g. vinyl flooring or floor tiles and possibly one of the models is better suited for the purpose. The measurement wheels have different coatings as can be seen in Figure 4.3. Coating of the left wheel is smooth Vulkollan plastic. Vulkollan plastic is suited for measuring on cardboard, wood, plastic, paper and wire surfaces. The right wheel has smooth Hytrel plastic coating that can be used for measuring on cardboard, wood, plastic and paper surfaces. [50]

Circumference of both measurement wheels is 0.5 m. The wheel models can be mounted on encoder shafts whose diameter is 10 mm. Screws are used for securing the wheels to the shafts. [50]

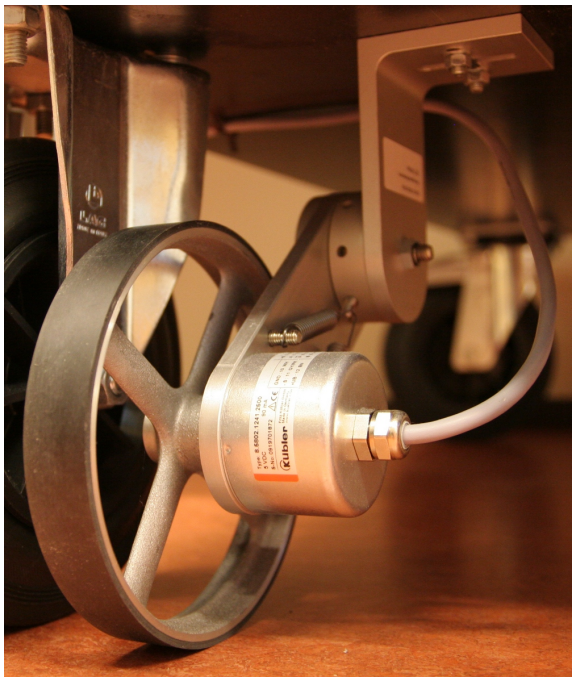

Figure 4.5. *Spring arm with the encoder and the left measurement wheel*

4.2.6 Spring Arms

Spring arms are used for mounting the encoders with the measurement wheels. They ensure that measurement wheels have good contact with the floor despite of possibly uneven surface. Two springs are used in spring arms to keep the measurement wheels under pressure. The spring pressure is adjustable from under 20 N to 40 N [51].

The left spring arm can be seen in Figure 4.5. It has been mounted under the plywood board next to the fixed left wheel to the back of the cart. The encoder has been mounted to the arm using screws.

4.2.7 Counter for the Encoders

To measure travelled distance of the cart, the steps of the encoders must be counted. USB4 encoder data acquisition USB device [52] by US Digital was selected to be used as counter for the encoders. The USB4 can record data from four encoders, eight digital inputs and four analogue inputs. In addition to recording the device has also eight digital and four analogue outputs.

The encoders have differential outputs, which is why the USB4 device model with differential encoder support (USB4-D) was selected. The device has a 24-bit up/down counter for every encoder input. Data acquisition can be triggered using digital, analogue or PWM (pulse-width modulation) input signals. The device also supports combinations of conditions in the input ports to form the final trigger. When triggering occurs the value of the time stamp counter, the counts of the four encoder inputs, and digital and analogue

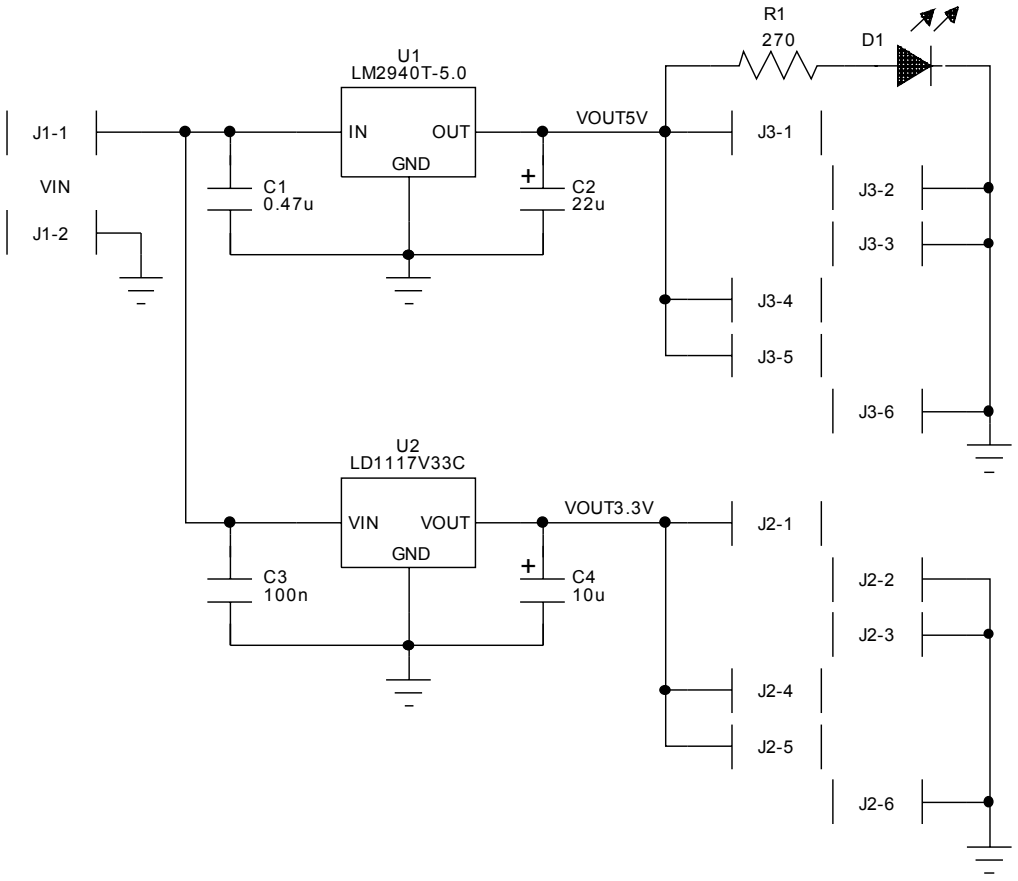

Figure 4.6. *The circuit diagram of the power supply*

input values are stored as a data packet to the memory of the device. The time stamp counter is a free running 32-bit counter that is clocked at 48 MHz. There is enough memory to store 800,000 data packets. The data packets can later be read from the memory to a computer using USB connection of the device. [52, 53]

The supply voltage of the counter can be from 8 V to 25 V. Its current usage is 77 mA when supply voltage is 12 V. In order to be correctly interpreted by the USB4 device, the high level voltage of the digital input signals must be at least 2 V and low level can be at maximum 0.8 V. [52]

4.2.8 Power Supply and Batteries

Rechargeable batteries provide power to the devices in the system. The counter for the encoders uses a 12 V battery as its power source. A 7.2 V battery is connected to a power supply that provides 3.3 V and 5.0 V supply voltages. The encoders take their 5.0 V supply voltage from the power supply. The power supply also provides 3.3 V and 5.0 V supply voltages for the gyro. The power supply can be seen in Figure 4.2.

The circuit diagram of the power supply can be seen in Figure 4.6. It uses two linear regulators to provide stable 3.3 V and 5.0 V supply voltages. Both regulators are low

dropout (LDO) voltage models meaning that the difference between the input and the output voltages of the regulators can be small. To provide a 5.0 V supply voltage an LDO regulator is needed because input voltage of the linear regulator from the battery is only 7.2 V. Model of the 5.0 V regulator is LM2940T-5.0. Its dropout voltage is typically 0.5 V and at maximum 1.0 V, thus typically a 5.5 V input is enough for the regulator to work properly and at maximum it needs 6.0 V [54]. Model of the 3.3 V regulator is LD1117V33C. Its dropout voltage is typically 1.0 V and at maximum 1.1 V, when output current is 100 mA [55].

The power supply is capable of supplying a 1 A current from its 5.0 V output [54]. The 3.3 V output can supply a 0.8 A current [55]. Cooling is needed for the regulators in order to prevent overheating on big loads. Both regulators have a heat sink to cool them down.

The connectors for the input and the outputs of the power supply are screw terminal blocks. They enable easy connection of devices. There are three output terminals for both 5.0 V and 3.3 V supply voltages. The power supply has an LED to indicate that it is powered on.

5. SYSTEM SOFTWARE

The system uses a data acquisition program to collect data from the sensors. The program runs on the laptop computer that also controls the USB-SPI interface and the counter for the encoders. Synchronisation of the sensors is achieved using the program to control a digital output of the USB-SPI interface and triggering properties of the counter for the encoders.

The position estimation is done in post processing. The collected sensor data is fed to a MATLAB program that estimates the position using the dead reckoning principle. Dead reckoning requires knowledge of the initial position for which a floor plan and a measuring tape is used.

5.1 Data Acquisition

A program running in Windows XP controls the data acquisition from the sensors. The program has been written using C and C++ languages. Manufacturer provided application programming interfaces (APIs) are used in the program to communicate with the USB-SPI interface and the counter for the encoders.

A flowchart of the program can be seen in Figure 5.1. The start up phase of the program is marked using blue colour in the figure. The main loop that acquires data from the sensors and saves it to log files is marked using grey colour. The end procedure of the program is marked using orange colour in the figure.

The data acquisition program starts by opening log files for saving data from the sensors. The data is saved in a binary format to separate files. By using a binary format the data takes less space than if it was saved using human readable ASCII (American Standard Code for Information Interchange) format. Binary data is also faster to read in post processing than ASCII data. Data from each sensor is saved to a separate file to make reading of the data easier in post processing. Each log file has, in addition to sensor data, a time stamp from the computer and encoder log files have also a time stamp of the counter for the encoders.

Before data collection from the sensors begins, connections to the USB-SPI interface and the counter for the encoders are opened and initialised. The accelerometer needs an initialisation procedure that is executed after opening the connection to the USB-SPI interface.

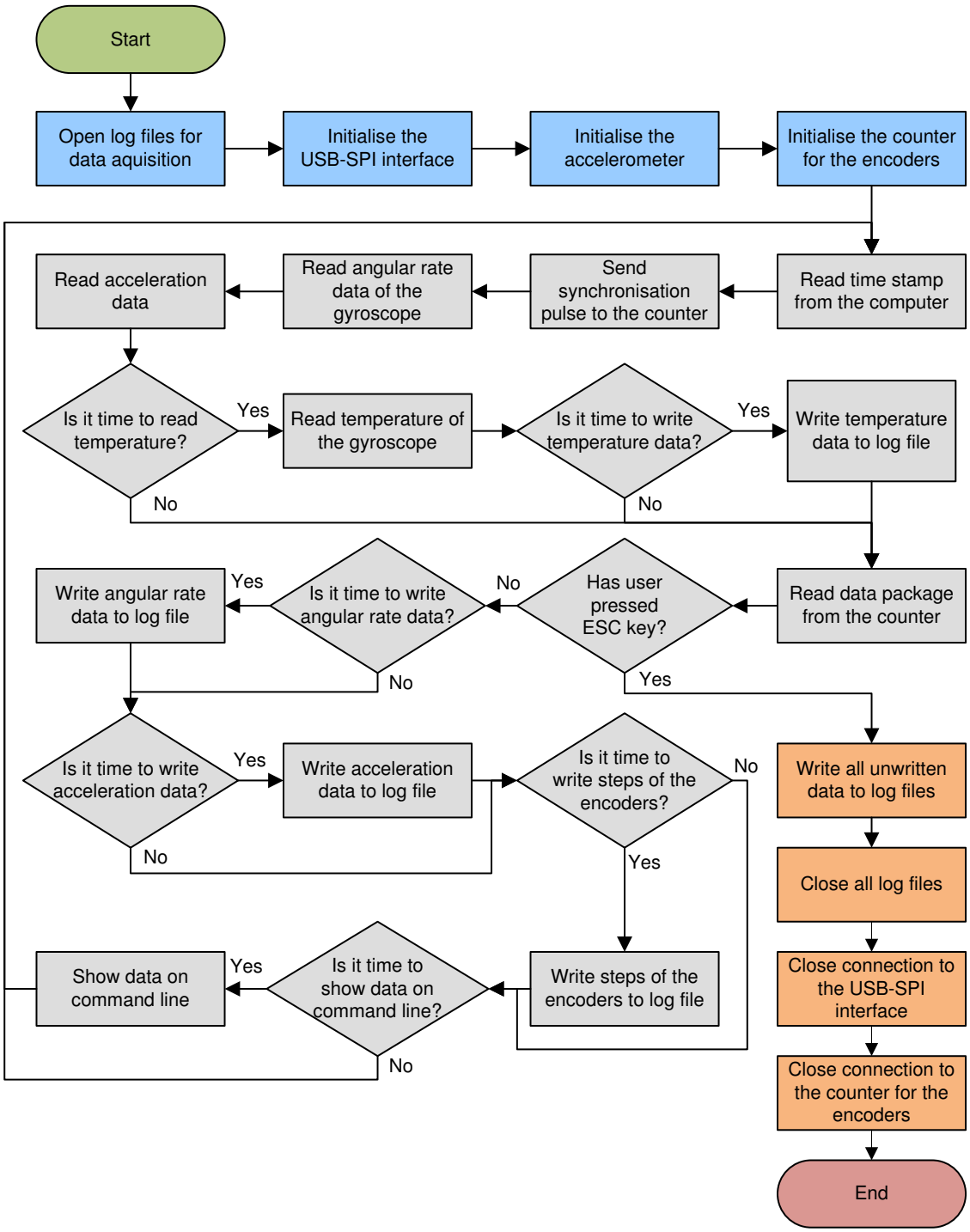

Figure 5.1. *Flowchart of the data acquisition program*

The data acquisition part of the program begins by reading the time stamp from the computer. After reading the time stamp, a synchronisation pulse from the USB-SPI interface is sent to the counter for the encoders. The pulse triggers the counter to save a data package to its internal memory. The package has, among other things, the counted steps of the encoders and the time stamp from the counter. The program continues by reading angular rate of the gyroscope and acceleration. The temperature of the gyro is not read on

every iteration of the main loop. The reading interval of the gyro temperature can be set with a command line parameter. If it is time to read the temperature the program reads it. When enough temperature measurements have been read, they are written to a log file.

Next the data package that was saved to the internal memory of the counter is read to the computer. After reading the package the program checks if user has pressed ESC key. If ESC key was pressed the program stops logging, saves the read data, closes all data files, closes connections to the devices and exits. If user did not interrupt the program the main loop continues and saves the data from the gyroscope, accelerometer and encoders to corresponding log files in case enough measurements have been received. Data from the encoders is found from the data package that was read from the counter together with a time stamp from the counter. Sensor data is not saved to the log files on every iteration of the loop, but it is saved to variables for later writing to the files. If the set interval has passed data is also printed to command line in text format. The purpose of showing the data on command line is to show the user that data acquisition is working.

Sampling rate of the sensors is approximately 100 Hz. The sensors are sampled as fast as possible in the data acquisition loop. Sampling rate is not constant because the computer is also running other programs at the same time. To overcome this problem, the samples are timestamped.

5.2 Synchronisation

The data acquisition program collects data from the SCC1300 sensor (angular rate, acceleration and temperature) and the counter for the encoders. In this system the data can not be collected from every sensor at exactly the same time. This limitation comes from the fact that angular rate, acceleration and temperature data from SCC1300 sensor must be read one after other. The other limiting factor is that the counter for the encoders can not be triggered at the same time as the SCC1300.

The synchronisation is not perfect in this system but it is good enough for the purpose. Requirement for the synchronisation is that the time difference between the synchronisation signal and angular rate reading is not more than half of the sampling interval of the system. As described in the previous section, a time stamp from the computer is saved just before sending a synchronisation pulse to the counter for the encoders. The pulse triggers the counter to save a data package to its internal memory that has, among other things, the value of the time stamp counter. The time between overflows of the time stamp counter is approximately 89.5 seconds [53]. The overflow condition happens so rarely that there is no risk of two overflows happening between two consecutive runs of the main sampling loop.

The time stamp from the computer used in the program has poor resolution. The resolution is typically in the range of 10 ms to 16 ms and it is too inaccurate to be used for position estimation [56]. Resolution of the time stamp counter must be better than 10 ms

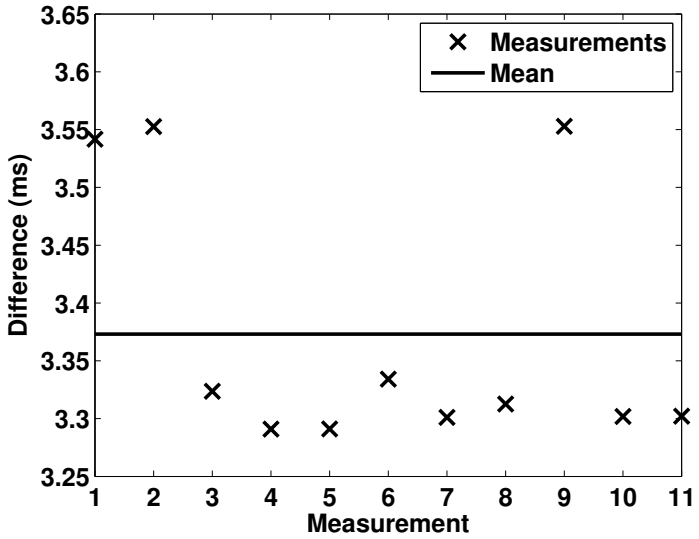

Figure 5.2. *Time difference between the synchronisation pulse of the counter for the encoders and triggering of the angular rate data*

in the system because it is used for time stamping data that has approximately 100 Hz sampling rate. The time stamp counter in the counter for the encoders has approximately 21 ns resolution, thus it is suitable for the purpose [53]. Even though the resolution of the time stamp from the computer is poor, it can still be used to check overflow conditions of the time stamp counter in the counter for the encoders.

Time difference between the synchronisation pulse and triggering of angular rate data of the gyroscope was measured using an oscilloscope. The triggering time of the angular rate data is unknown. In the measurements, triggering was thought to happen when the parity bit in the end of read angular rate command was send through SPI. This was thought to be the best approximation for triggering of the angular rate data, since the internal operation of the gyroscope is not known. After the end of read angular rate command the gyroscope gives out its angular rate data. The data starts from the next clock cycle of SPI and thus it must be triggered before or at the end of the read command.

The synchronisation pulse and triggering of the angular rate data was measured to have 3.37 ms time difference on average. Eleven measurements were performed to find out the difference. The measurements can be seen in Figure 5.2 together with their mean value. The minimum measured time difference was 3.29 ms and the maximum was 3.55 ms, thus the maximum deviation from the mean value was 0.18 ms. Standard deviation of the measurements was 0.11 ms.

One of the time difference measurements can be seen in Figure 5.3. In the figure the *cs_g* signal is the chip select of the gyroscope, *sync* is the synchronisation pulse signal, *mosi* is the data sent from the computer to the gyroscope and *sck* is the clock of the SPI bus. In Figure 5.3a, start of the synchronisation pulse can be seen on the left in the place

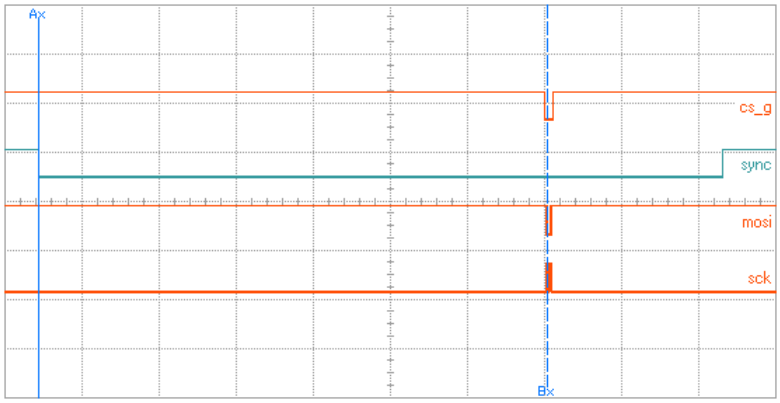

(a) *The whole measurement. The Ax marker is in the start of the synchronisation pulse. Scale of the horizontal axis is* 500 µs/div.

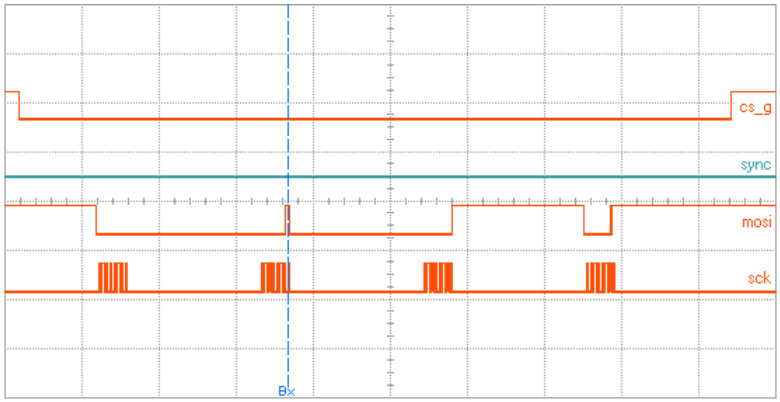

(b) *SPI communication with the gyro, zoomed in from the figure above. Scale of the horizontal axis is* 5.00 µs/div.

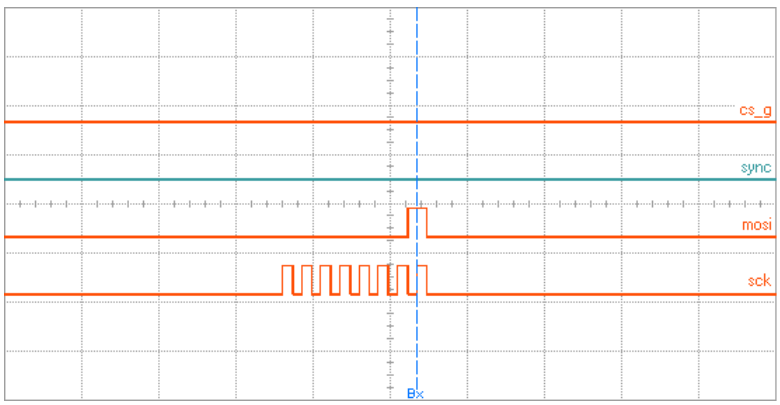

(c) *Last part of the read angular rate command, zoomed in from the figure above. The Bx marker is in the place starting from which the gyro can read the parity bit of the read angular rate command. Scale of the horizontal axis is* 1.00 µs/div.

Figure 5.3. *A triggering time difference measurement. Scale of the vertical axis in every figure is* 5 V/div.

of the Ax marker. SPI communication with the gyroscope can be seen near the Bx marker. Figure 5.3b shows a closer view of the SPI communication shown in Figure 5.3a. The Bx marker has been placed to the last bit of the read angular rate command, that is the parity

bit. To be more precise the Bx marker has been placed on a rising edge of the serial clock signal's pulse. The rising edge of the pulse is in the place starting from which the parity bit is readable by the gyro [47]. A close view of the parity bit and the clock pulse can be seen in Figure 5.3c. The difference between the triggering of the counter for the encoders and the angular rate data is the time between the markers Ax and Bx.

5.3 Position Estimation

The position of the system is determined using the dead reckoning principle. Angular rate from the gyro and steps from the encoders are used for navigation. Dead reckoning computation needs an initial position. Initial coordinates for the computation are $x_0 = 0$ and $y_0 = 0$. In addition to coordinates, an initial heading $\psi_0 = 0^\circ$ is also needed. The heading is propagated using equation 2.3 for which the acquired angular rate is used. After the heading has been updated, the coordinates are propagated using equation set 2.5. The travelled distance obtained from the steps of the encoders and the updated heading is used for propagating the coordinates.

The position estimation is done in post processing using MATLAB running on a PC. As described earlier in section 5.1, the angular rate data and steps of the encoders are saved to files during data acquisition. Data of the files is used now for position estimation.

The dead reckoning computation includes the following steps:

1. The counted steps of the encoders and time stamps from the counter for the encoders are read from log files. Step counts are 24 bit and time stamps 32 bit unsigned numbers [53]. They are unwrapped and the time stamps are converted to seconds. Unwrapping enables numbers to have greater or smaller values than representable using a fixed bit amount. In addition to time stamps from the counter, time stamps were also obtained from the PC clock. The PC time stamps are used to make sure that unwrapping the counter time stamps is working properly. Unwrapped time stamps from the counter are used to time tag encoder counts and angular rate data. The measured mean value of the trigger time difference could be used to correct timing of the gyroscope but to make position estimation easier the gyro time stamps were not corrected.

2. Encoder counts are used to find times when the system has been stopped. This is done by differentiating counts of both encoders separately and taking absolute values of those. If the sum of the absolute values at an instant is zero, the system is considered to be stationary.

3. For every stop lasting at least 25 seconds, bias of the gyroscope is calculated as mean value of angular rate data collected during the stop.

4. Counts of the encoders are converted to travelled distance using circumferences of the wheels and encoders' number of steps per revolution. After conversion, the distance of the left wheel is corrected using the scale factor calculated in the calibration of the encoders. Travelled distance of the system is calculated as the mean of the distances by left and right wheel to estimate the distance correctly even on turns when the wheels measure different distances.

5. Biases during stops are subtracted from angular rate. The calculated mean bias of a stop is used for angular rate data from the start of a stop until the start of the next stop. Then angular rate is converted to $^\circ/\mathrm{s}$ using different scale factors for positive and negative values. The scale factors are obtained from a calibration of the gyroscope that is done just before the system is used for positioning.

6. Heading is obtained using equation 2.3. In the equation, the converted angular rate is integrated with respect to time obtained from the counter for the encoders. The aforementioned initial heading $\psi_0 = 0^\circ$ is used in the calculation.

7. Position estimates are obtained from heading and distance estimates using equation set 2.5. The aforementioned initial position $x_0 = 0$ and $y_0 = 0$ is used in the computation.

6. EXPERIMENTS AND PERFORMANCE ANALYSIS

The positioning performance of the system was analysed in a test drive. The system was attached to a cart and driven indoors along corridors. Before the test drive error sources of the gyroscope and the encoders were analysed and both were calibrated. Calibration of the gyroscope was needed just before the test drive to minimise errors in heading estimates.

6.1 Calibration Procedure

Before analysing positioning performance of the system, the error sources of the gyroscope and encoders were analysed to figure out needed calibration. Error sources of the gyroscope were studied using a turn table. Distance measurement errors of the encoders were found out in straight line driving tests.

6.1.1 Gyroscope

The most significant error sources of a gyroscope are bias and scale factor error. Bias causes an error that remains regardless of the angular rate, while scale factor error depends on the sensed angular rate. These both were studied using a turn table.

The gyroscope was attached to a Velmex B5990TS [57] turn table and it was rotated at different angular rates to study the scale factor. The turn table with the gyroscope can be seen in Figure 6.1. The angular rates used in the study were 5, -5, 10, -10, ..., 40 and -40. The gyroscope was rotated 720 degrees with each angular rate value. Positive and negative angular rates were rotated alternately to prevent the wires going to the gyroscope from turning too much to one direction. Before every angular rate measurement, the table was kept still for 60 s to estimate the gyroscope bias. The bias was removed from angular rate data and the scale factors were estimated using the equation 3.1. Cross-coupling errors were assumed to be zero in the equation to obtain the scale factor estimates. The turn table does not provide information of its actual angular rate, so it was assumed to be rotating at programmed rates.

The scale factor study was repeated on six different days and the results can be seen in Figure 6.2. Variation was significant with this prototype sensor from day to day. The variation is however within the total scale factor error ± 2 % given in the data sheet [46].

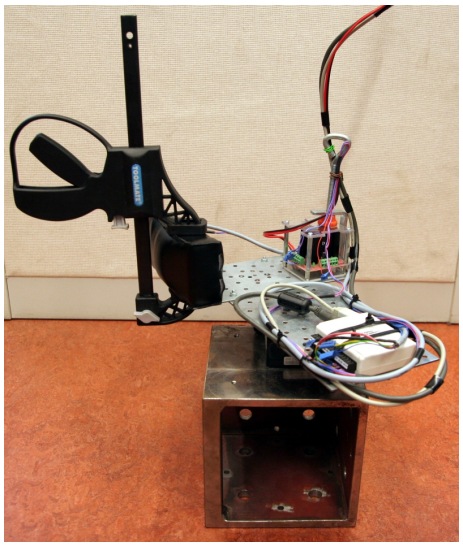

Figure 6.1. *The gyro with the USB-SPI interface and power supply on the turn table*

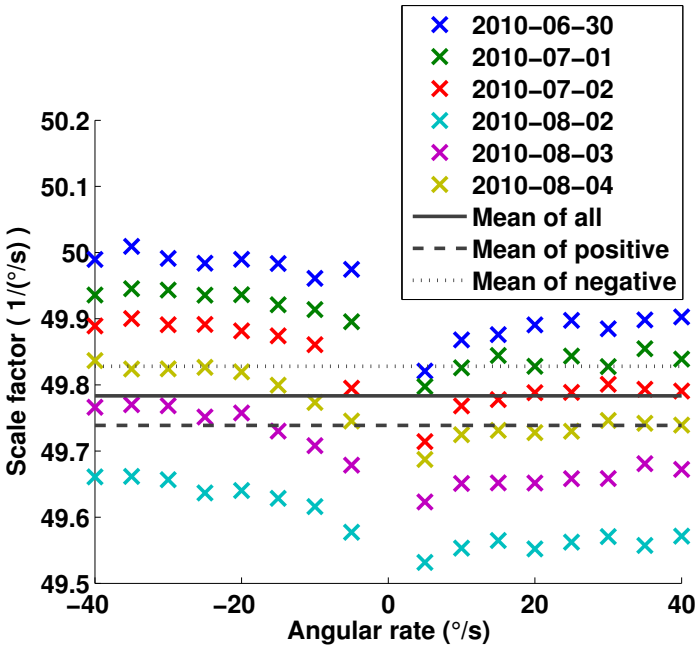

Figure 6.2. *Gyroscope scale factors obtained using the turn table*

Scale factors for positive and negative angular rates were slightly different. The difference between the mean values of positive and negative scale factors was approximately $0.09/(^\circ/\mathrm{s})$. The biases measured between rotations can be seen in Figure 6.3. It can be seen that the gyro temperature has not been the same in all studies, but it has been quite stable during each of the studies. The bias has changed significantly not only between the studies but it has also varied during the studies.

It became obvious from the studies that for positioning performance analysis, the gyro scale factor and bias calibrations need to be done just before test drive of the system.

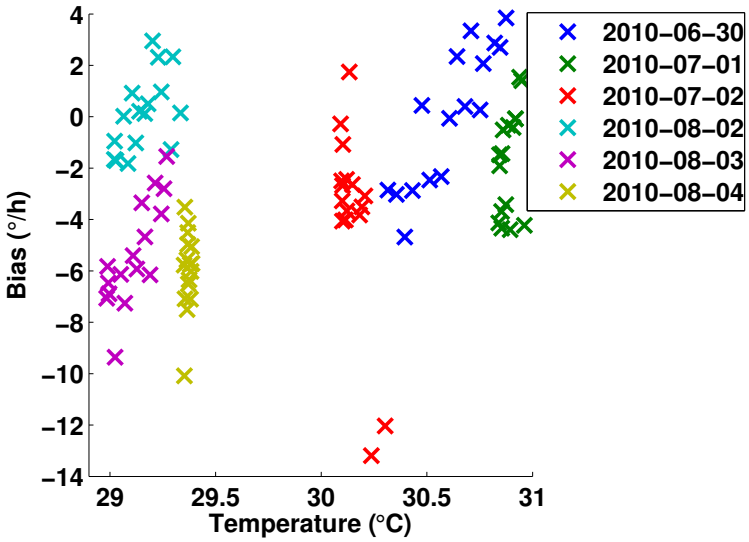

Figure 6.3. *Gyroscope biases from turn table measurements*

6.1.2 Encoders

The distance measurement accuracy by the wheel encoders was tested by driving the positioning cart in a straight line. Measurements were done by driving the positioning cart along a corridor. It was driven a 24.226 m distance several times, following as straight a line as possible. This reference distance measurement was done using a 50 m measuring tape that can be seen in Figure 6.4. The distance measurements from the drives based on encoders are shown in Figure 6.5.

The difference between average measurements of right measurement wheel and the measuring tape was only about 2 mm. This corresponds to about 0.008 % error in travelled

Figure 6.4. *Measuring tape used as distance reference in straight line measurements*

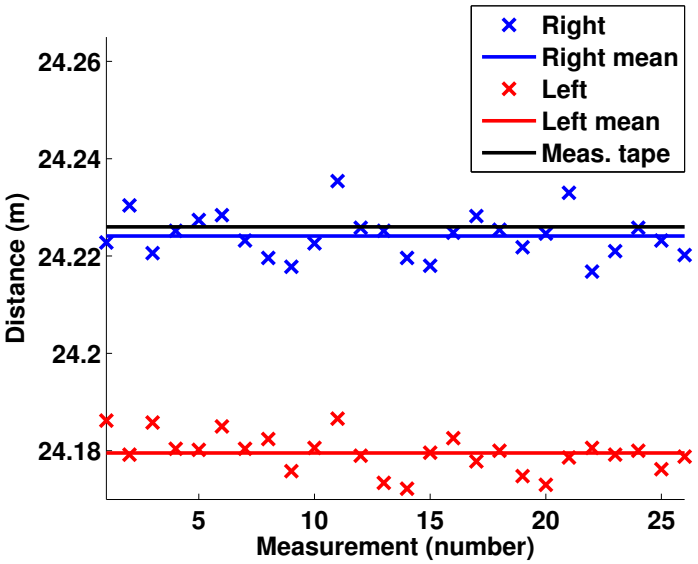

Figure 6.5. *Wheel encoder straight line distance measurements*

distance. The standard deviations of distances by right and left measurement wheels were 5 and 4 mm, respectively.

The distances obtained by left wheel on average are about 46 mm less than distances by right wheel. Small differences in wheel diameter cause this difference, which introduces a scale factor difference between the wheels. This can be seen in the instantaneous difference in distance readings of the wheels shown in Figure 6.6. The difference grows linearly as a function of the right wheel measurement, although a significant amount of noise can be seen in the curves. The noise is caused by small bends on the track, as

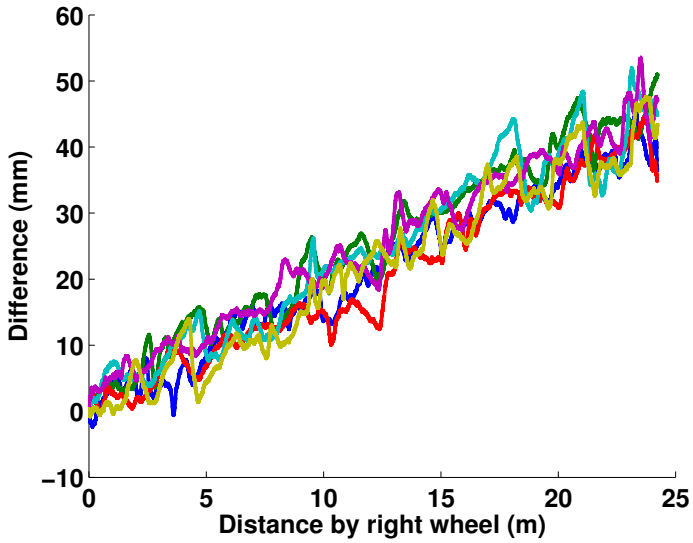

Figure 6.6. *Distance difference between the wheels in straight line distance measurements*

keeping the straight line course during the drives was quite a challenging task. Based on these measurements a scale factor was calculated for the left wheel. The distance from left wheel was multiplied by 1.001857 in position estimation to compensate the difference between the wheels.

6.2 Calibration of the Gyroscope During the Test

The scale factor of the gyroscope was calibrated for the test drive just before the actual test drive began. The gyroscope was attached to the positioning cart and the cart was turned three circles. At the start and the end of the turning the cart was placed against a wall. By placing the cart against a wall the gyroscope could be aligned to get an accurate rotation of three circles. This measurement was repeated three times clockwise and counterclockwise. The data from about 60 s before turning the cart was used to estimate the gyroscope bias. Scale factors calculated from these measurements can been seen in Figure 6.7.

Scale factors for positive and negative angular rates were obtained as mean values of scale factor estimates of the corresponding direction. The obtained scale factor for positive and negative directions were $49.62/(^\circ/\mathrm{s})$ and $49.72/(^\circ/\mathrm{s})$, respectively. Their difference, $0.10/(^\circ/\mathrm{s})$, is close to the difference obtained in the turn table calibration.

Gyroscope bias was estimated during the test drive always when the cart was stopped for period longer than 25 s, and the most recent bias estimate was used to compensate the gyroscope bias. Encoder counts were used for detecting the stops; if the count didn't change, it was considered that the cart was stopped.

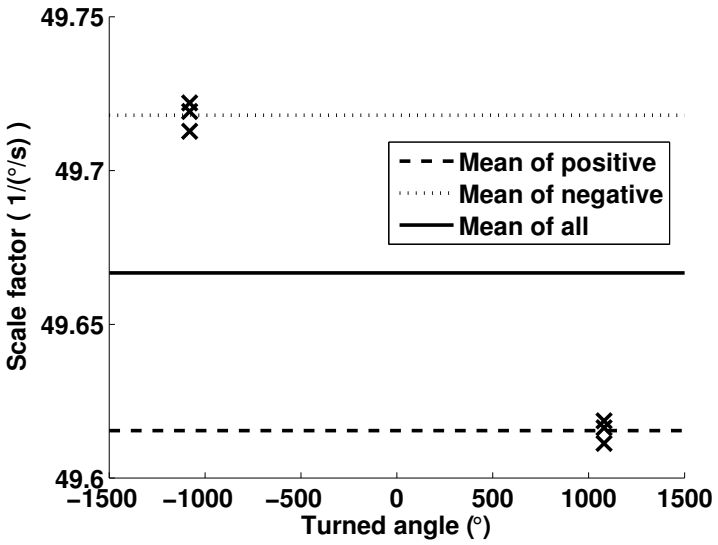

Figure 6.7. *Scale factors from cart measurements*

6.3 Driven Test Route

Two dimensional positioning accuracy of the system was tested by driving the positioning cart indoors. According to the dead reckoning principle the position estimation needs to be started from a known position. The starting position was selected with the help of a floor plan and it was set to be the origin of coordinates. In this case the coordinate system uses local coordinates instead of global coordinates.

In the test, the positioning cart was driven seven times back and forth along a route seen in Figure 6.8. The route started and ended in the left corridor of the figure. It does not test the worst case accuracy of the system, as the cumulative turn angles to opposite directions are equal, and therefore the accumulation of position errors caused by the gyroscope scale

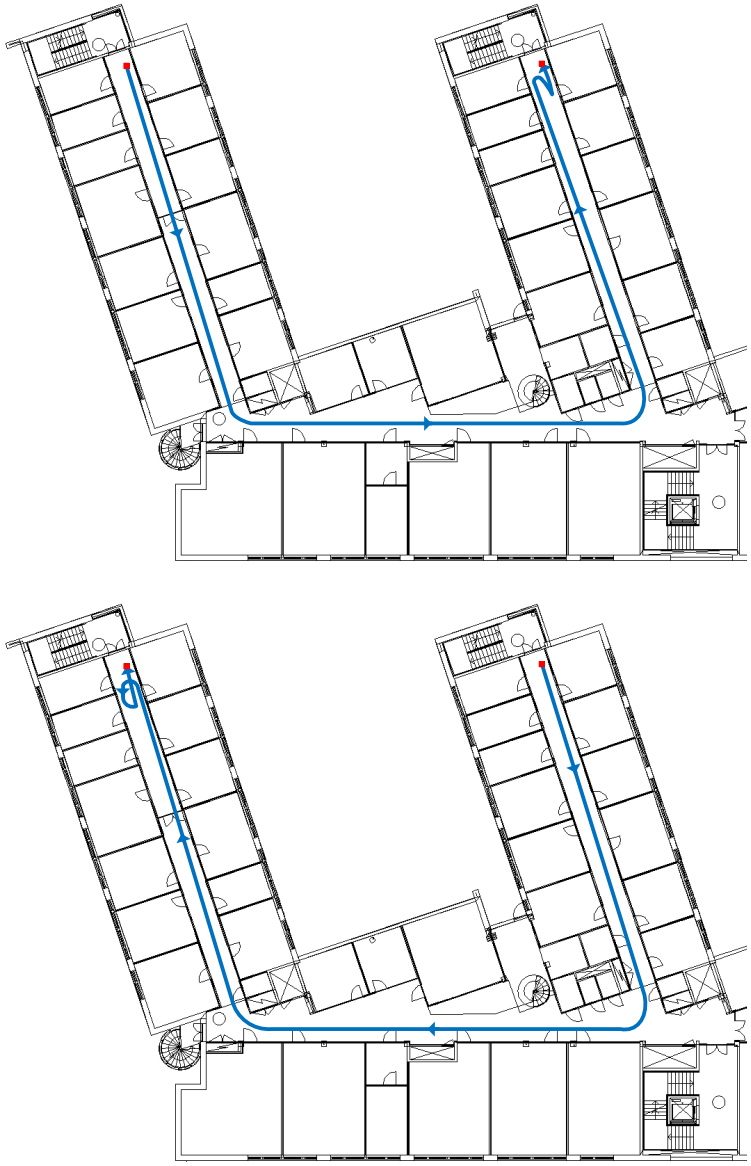

Figure 6.8. *Test drive route. Start of the route is above and end is below.*

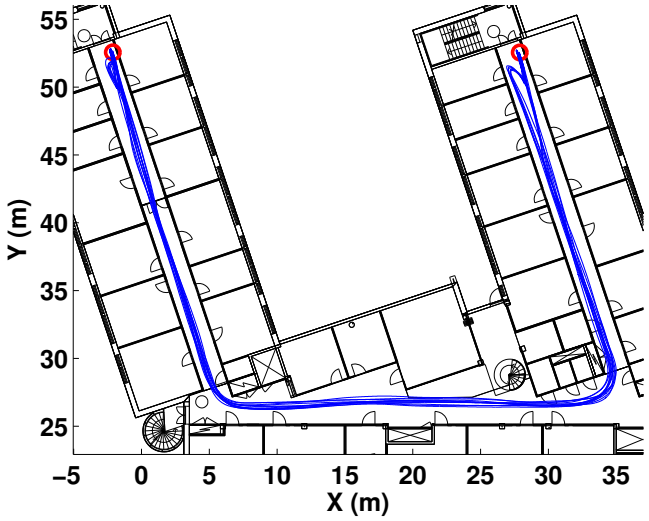

Figure 6.9. *Estimated track on floor plan, red circles indicate reference locations*

factor is minimised. However, this choice is justifiable, as for example, in radio map measurements the user can optimise the measurement route to obtain the best possible accuracy for the reference measurements provided by the system.

On each pass, the cart was stopped at the known locations at the end of corridors, where the estimated position can be compared to reference coordinates. During the stops it was placed against the wall to align the gyro with the corridor in order to test also the heading accuracy. The reference coordinates were obtained using the floor plan and a measuring tape. The reference points, marked using red squares, can be seen in Figure 6.8. Along the route, the correctness of the position estimates could be assessed by comparing the computed track to the floor plan.

6.4 Estimated Track

The estimated track has been computed using the procedure presented in the Position Estimation section. It can be seen in Figure 6.9. Based on these results, the estimation is accurate enough at least in the scale of the corridors. The position estimates on reference locations were compared with their known coordinates and the results are shown in Figure 6.10. In the figure, the total error distances between the reference and the estimated coordinates are shown together with the errors of both coordinates. The total errors can be seen to stay below 30 cm on the test drive that lasted 30 minutes. It is expected that the total positioning error will grow when the system is used for longer time because errors of the sensors accumulate in the position estimates. During the drive the gyro bias was corrected whenever the system was stopped in the reference locations. The bias corrections improved the positioning accuracy in comparison to using only one bias value for the test drive. The route was also optimised to minimise errors caused by the gyro

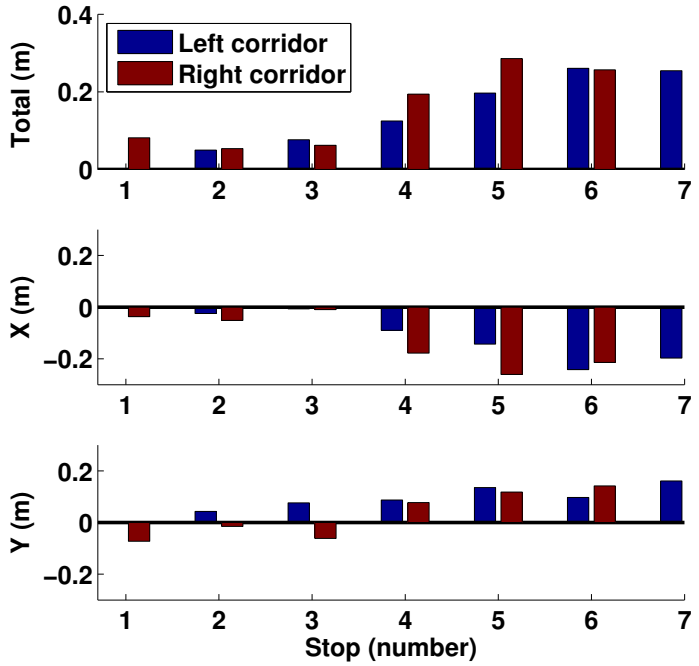

Figure 6.10. *Positioning error in reference locations*

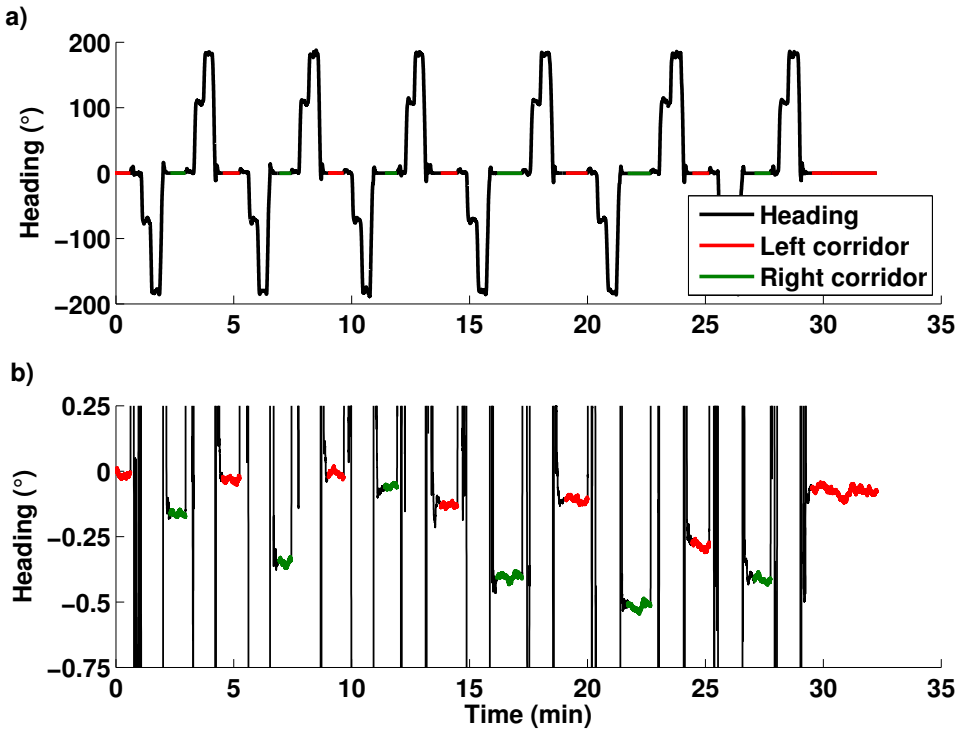

Figure 6.11. *a) Estimated heading, b) Estimated heading around 0°, zoomed in. Stops in reference locations are indicated by colors; red: left corridor reference, green: right corridor reference.*

scale factor. The gyro scale factor errors are minimised because the route has equal turn angles to both directions.

The accuracy of the gyroscope was analysed using heading estimates of the test drive. Because the left and right corridors (shown in Figures 6.8 and 6.9) are in the same angle with each other, the accuracy of the gyroscope can be analysed by comparing the heading estimates in the aligned corridors. With an ideal gyroscope the headings should be the same; the performance of the gyroscope can be assessed by studying the deviation of the estimated angle from the ideal 0° in the reference locations. The heading estimates on the reference locations are shown in Figure 6.11 a) and in Figure 6.11 b), where the heading range observed on reference locations is zoomed in. From these figures it can be seen that the heading error stays below 0.5° for the test drive. It can also be noticed that during the stops in the reference locations, the drift of the heading is quite small, as the bias reset has been applied in the beginning of the stop.

7. CONCLUSIONS

In this thesis a dead reckoning system was implemented and its performance was analysed. The system uses wheel encoders to measure the travelled distance and a prototype MEMS gyro to obtain the heading. The encoders are connected to a counter to obtain the travelled distance. The gyro is connected to a USB-SPI interface for communication with a laptop computer. The USB-SPI interface also sends pulses to trigger the counter. The computer is used to acquire data from the counter of the encoders and the gyro to the data files. The files are used in post processing to estimate position of the system. It has been mounted on a cart for easy transportation that can be also used to carry other possible measurement devices.

The accuracy of the gyro was studied using a turn table before the accuracy of the complete system was tested. The gyro was rotated at several different angular rates both clockwise and counterclockwise to study behaviour of its scale factor. Its bias was estimated before every rotation. The study was repeated on six different days. It was found out that the gyro has different scale factors for positive and negative angular rates and their day to day variation is significant. The bias was found out to be varying not only between studies on different days but also within a study. Gyro bias depends on temperature history [58], that makes it hard to compensate the effect of temperature on measurements. The temperature effect on the gyro bias was not compensated in the system but the gyro was insulated to minimise temperature changes. In order to have as stable temperature during the measurements as possible, the gyro was powered on some time before using it allowing the temperature to stabilise. It became obvious from the studies that the gyro scale factor and the bias needed to be calibrated just before the system was used for positioning.

The accuracy of the wheel encoders was studied in straight line measurements. The encoders were mounted to the cart and it was driven approximately a 25 meter distance several times. Right wheel encoder was found out to be having only 0.008 % error in the travelled distance whereas the left wheel distance readings had much larger errors. Standard deviations of the distances for right wheel and left wheel were respectively 5 and 4 mm. A linear dependency was found by studying instantaneous differences in the distance readings. This dependency is the result of small differences in wheel diameters. A scale factor for the left wheel encoder was calculated to compensate the difference between encoder readings.

The positioning accuracy of the system was studied in a test drive. Before the test began the gyro was rotated three turns clockwise and counterclockwise, repeating the measurement three times, to calibrate its scale factor for positive and negative angular rates. The difference between the obtained scale factors for positive and negative angular rates were found to be close to the ones obtained in the turn table studies. The gyro bias was recalibrated during the drive when the system was stopped. On the test drive lasting 30 minutes a positioning accuracy of better than 30 cm was achieved. During the drive the system was stopped 13 times for duration of approximately 30 seconds to estimate the gyro bias. The positioning accuracy might improve by replacing the prototype gyro with a production version. Nevertheless, the positioning error of the system was smaller than the required 1 m when the system was used for 30 minutes. Thus it is suitable for setting up fingerprinting systems and it can be used as a reference for other indoor positioning systems. Dead reckoning systems with low-cost MEMS gyros seem to be reasonable candidates for accurate indoor positioning.

Sampling rates of the sensors were found to be varying in the system. The data acquisition from the sensors is done as fast as possible using the computer that runs Windows XP. The operating system runs also other processes than the data acquisition software and hence the running speed can not be guaranteed to be constant. More accurate sampling rates might be achievable by changing the acquisition program to use concurrency as much as possible. Accurate sampling could be achieved by using a real-time operating system to run the acquisition. Real-time operating systems are designed to handle steady flows of information, for example to sample sensors, without interruption. Changing to a real-time operating system would most likely require hardware changes as the USB devices of the current system are not designed for real-time system usage. A computer system specially designed for the purpose, also known as an embedded system, could be designed to run the acquisition. In the embedded system, all the sensors could be directly connected without the USB devices. Better accuracy in sampling rates might result in improved positioning accuracy. In the current system the heading is obtained by integrating angular rate of the gyro. When there is a turn in a track the angular rate may change a lot between samples causing errors in heading if the sampling rate is not high enough. At least more accurate sampling would make the position more reliable on tracks having a lot of turns.

The time difference between triggering of the counter for the encoders and the gyro was found out to be 3.37 ms on average. As the sampling rate of the system is approximately 100 Hz the difference corresponds to about 34 % of the sampling interval. If the difference could be made smaller, the sampling rate of the system might increase and improve the positioning accuracy. Smaller triggering time difference might also improve the accuracy even though the sampling rate would not increase. Currently the same time stamps are used for the encoders and the gyro and having smaller triggering difference would make

those more accurate. One option to decrease the difference would be to use the chip select signal of the gyro's SPI bus as a synchronisation pulse for the counter. The signal goes down in the beginning of communication and changes back to high after it. The problem in using the chip select signal is that triggering of the counter would only be needed when angular rate is read. In addition to angular rate reading, the bus is also used to read acceleration and temperature. Triggering could be set to happen whenever there is a falling edge in the chip select signal, indicating start of communication, but that would require filtering out unwanted encoder data packages resulting from using the bus to read temperature and acceleration.

REFERENCES

[1] Leppäkoski, H., Tikkinen, S., Takala, J. Optimizing Radio Map for WLAN Fingerprinting. Proceedings of the Ubiquitous Positioning Indoor Navigation and Location Based Service (UPINLBS), 2010. Helsinki, Finland, 2010, pp. 1–8.

[2] Perez Iglesias, H., Barral, V., Escudero, C. Indoor Person Localization System Through RSSI Bluetooth Fingerprinting. Proceedings of the 19th International Conference on Systems, Signals and Image Processing (IWSSIP), 2012. Vienna, Austria, 2012, pp. 40–43.

[3] Misra, P., Enge, P. Global Positioning System: Signals, Measurements, and Performance. Ganga-Jamuna Press, 2006, 2nd edition.

[4] Groves, P.D. Principles of GNSS, Inertial, and Multisensor Integrated Navigation Systems. Artech House, 2008.

[5] Inertial Navigation. [WWW]. VectorNav Technologies. Available from: `http://www.vectornav.com/support/library?id=76` [cited 31 August 2013].

[6] Pekkalin, O., Leppäkoski, H., Iozan, L., Hautamäki, J., Collin, J., Takala, J. Reference for Indoor Location Systems Using Gyroscope and Quadrature Incremental Encoder. Proceedings of the ION GNSS 2010, 23rd International Technical Meeting of the Satellite Division of the Institute of Navigation. Portland, OR, USA, 2010, pp. 1192–1197.

[7] Iozan, L.I., Collin, J., Pekkalin, O., Hautamäki, J., Takala, J., Rusu, C. Measuring the Earth's Rotation Rate Using a Low-Cost MEMS Gyroscope. Proceedings of the Symposium Gyro Technology 2010. Karlsruhe, Germany, 2010, pp. 20.1–20.16.

[8] Gabaglio, V. Centralised Kalman Filter for Augmented GPS Pedestrian Navigation. Proceedings of the ION GPS 2001, 14th International Technical Meeting of the Satellite Division of the Institute of Navigation. Salt Lake City, UT, USA, 2001, pp. 312–318.

[9] Käppi, J., Syrjärinne, J., Saarinen, J. MEMS-IMU Based Pedestrian Navigator for Handheld Devices. Proceedings of the ION GPS 2001, 14th International Technical Meeting of the Satellite Division of the Institute of Navigation. Salt Lake City, UT, USA, 2001, pp. 1369–1373.

[10] Jin, Y., Toh, H.S., Soh, W.S., Wong, W.C. A Robust Dead-Reckoning Pedestrian Tracking System with Low Cost Sensors. Proceedings of the IEEE International Conference on Pervasive Computing and Communications (PerCom), 2011. Seattle, WA, USA, 2011, pp. 222–230.

[11] Collin, J., Mezentsev, O., Lachapelle, G. Indoor Positioning System Using Accelerometry and High Accuracy Heading Sensors. Proceedings of the ION GPS/GNSS 2003, 16th International Technical Meeting of the Satellite Division of the Institute of Navigation. Portland, OR, USA, 2003, pp. 1164–1170.

[12] Judd, T. A Personal Dead Reckoning Module. Proceedings of the ION GPS 1997, 10th International Technical Meeting of the Satellite Division of the Institute of Navigation. Kansas City, MO, USA, 1997, pp. 47–51.

[13] Ladetto, Q., van Seeters, J., Sokolowski, S., Sagan, Z., Merminod, B. Digital Magnetic Compass and Gyroscope for Dismounted Soldier Position & Navigation. Proceedings of the Military Capabilities enabled by Advances in Navigation Sensors, Sensors & Electronics Technology Panel, NATO-RTO meetings. Istanbul, Turkey, 2002.

[14] Leppäkoski, H., Käppi, J., Syrjärinne, J., Takala, J. Error Analysis of Step Length Estimation in Pedestrian Dead Reckoning. Proceedings of the ION GPS 2002, 15th International Technical Meeting of the Satellite Division of The Institute of Navigation. Portland, OR, USA, 2002, pp. 1136–1142.

[15] Ladetto, Q. On Foot Navigation: Continuous Step Calibration Using Both Complementary Recursive Prediction and Adaptive Kalman Filtering. Proceedings of the ION GPS 2000, 13th International Technical Meeting of the Satellite Division of The Institute of Navigation. Salt Lake City, UT, USA, 2000, pp. 1735–1740.

[16] Titterton, D.H., Weston, J.L. Strapdown Inertial Navigation Technology. The Institution of Electrical Engineers, 2004, 2nd edition.

[17] Kempe, V. Inertial MEMS: Principles and Practise. Cambridge University Press, 2011.

[18] Looney, M. A Simple Calibration for MEMS Gyroscopes. EDN Europe, (2010), July, pp. 28–31. Available from: `http://www.analog.com/static/imported-files/tech_articles/GyroCalibration_EDN_EU_7_2010.pdf` [cited 27 September 2012].

[19] Syed, Z.F., Aggarwal, P., Goodall, C., Niu, X., El-Sheimy, N. A New Multi-Position Calibration Method for MEMS Inertial Navigation Systems. Measurement Science and Technology, 18, 7, (2007), July, pp. 1897–1907. Available from: `http://iopscience.iop.org/0957-0233/18/7/016/pdf/0957-0233_18_7_016.pdf` [cited 29 September 2012].

[20] Groves, P.D. Principles of Integrated Navigation. [course notes]. QinetiQ Ltd, 2002.

[21] LPR410AL MEMS Motion Sensor: Dual-Axis Pitch and Roll ±100 dps Analog Gyroscope. [datasheet]. STMicroelectronics, October 2009. Available from: http://www.st.com/internet/com/TECHNICAL_RESOURCES/TECHNICAL_LITERATURE/DATASHEET/CD00254123.pdf [cited 15 June 2012].

[22] A3G4250D MEMS Motion Sensor: 3-Axis Digital Output Gyroscope. [datasheet]. STMicroelectronics, February 2012. Available from: http://www.st.com/internet/com/TECHNICAL_RESOURCES/TECHNICAL_LITERATURE/DATASHEET/DM00047823.pdf [cited 3 August 2012].

[23] Fiber Optic Gyro (FOG) Product Selector. [product selector]. KVH Industries, 2012. Available from: http://www.kvh.com/ViewAttachment.aspx?guidID={BC800C0A-AE05-41CB-BEB1-A1784C9E2AE9} [cited 3 August 2012].

[24] SRS 1000 User's Manual. [datasheet]. Optolink Scientific. Available from: http://www.optolink.ru/ftpgetfile.php?id=74 [cited 7 September 2012].

[25] Differential Signaling, Application Note AN6019. [application note]. Lattice Semiconductor, May 2001. Available from: http://www.latticesemi.com/lit/docs/appnotes/pac/an6019.pdf [cited 10 August 2012].

[26] A Quick Comparison of RS-232, RS-422, and RS-485 Serial Communication Interfaces. [WWW]. National Instruments, June 2010. Available from: http://digital.ni.com/public.nsf/allkb/2CABB3FD5CAF2F8686256F1D005AD0CD [cited 3 August 2012].

[27] Patrick, J. Serial Protocols Compared. [WWW]. UBM Electronics, May 2002. Available from: http://eetimes.com/design/embedded/4023975/Serial-Protocols-Compared [cited 7 August 2012].

[28] Kalinsky, D., Kalinsky, R. Introduction to Serial Peripheral Interface. [WWW]. UBM Electronics, February 2002. Available from: http://eetimes.com/discussion/beginner-s-corner/4023908/Introduction-to-Serial-Peripheral-Interface [cited 7 August 2012].

[29] Kalinsky, D., Kalinsky, R. Introduction to I2C. [WWW]. UBM Electronics, July 2001. Available from: http://eetimes.com/discussion/beginner-s-corner/4023816/Introduction-to-I2C [cited 9 August 2012].

[30] Uotila, P. Tietoliikenteen tekniikka, verkot ja protokollat. Talentum Media, 2001, 4th edition.

[31] RS232 Serial Interface Tutorial. [WWW]. Adrio Communications. Available from: http://www.radio-electronics.com/info/telecommunications_

networks/rs232/rs232-serial-interface-basics-tutorial.php [cited 21 August 2012].

[32] Selecting and Using RS-232, RS-422, and RS-485 Serial Data Standards, Application Note 723. [application note]. Maxim Integrated Products, December 2000. Available from: http://pdfserv.maxim-ic.com/en/an/AN723.pdf [cited 20 August 2012].

[33] Explanation of Maxim RS-485 Features, Application Note 367. [application note]. Maxim Integrated Products, December 2000. Available from: http://pdfserv.maxim-ic.com/en/an/AN367.pdf [cited 24 August 2012].

[34] Verplaetse, C. Can a Pen Remember What It Has Written Using Inertial Navigation?: An Evaluation of Current Accelerometer Technology. [WWW]. Available from: http://xenia.media.mit.edu/~verp/projects/smartpen [cited 9 February 2013].

[35] LIS332AR MEMS Motion Sensor: 3-Axis ±2 g Analog-output Ultracompact Accelerometer. [datasheet]. STMicroelectronics, February 2010. Available from: http://www.st.com/internet/com/TECHNICAL_RESOURCES/TECHNICAL_LITERATURE/DATASHEET/CD00259964.pdf [cited 7 September 2012].

[36] AIS326DQ MEMS Inertial Sensor: 3-Axis, Low g Accelerometer with Digital Output. [datasheet]. STMicroelectronics, June 2010. Available from: http://www.st.com/internet/com/TECHNICAL_RESOURCES/TECHNICAL_LITERATURE/DATASHEET/CD00207961.pdf [cited 7 September 2012].

[37] Digital Servo-Accelerometer High Performance: SX41800 Series. [datasheet]. Sensorex. Available from: http://www.sensorex.fr/upload/fiches_techniques/57-en-SX41800GB.pdf [cited 7 September 2012].

[38] Parviainen, J., Vázquez López, M.A., Pekkalin, O., Hautamäki, J., Collin, J., Davidson, P. Using Doppler Radar and MEMS Gyro to Augment DGPS for Land Vehicle Navigation. Proceedings of the MSC 2009, 3rd IEEE Multi-Conference on Systems and Control. Saint Petersburg, Russia, 2009, pp. 1690–1695.

[39] Radar III Ground Speed Sensor. [datasheet]. DICKEY-john, 2005. Available from: http://www.dickey-john.com/_media/11071-0313-200702%20_1.pdf [cited 18 September 2012].

[40] Rasshofer, R., Biebl, E. A Direction Sensitive, Integrated, Low Cost Doppler Radar Sensor for Automotive Applications. Proceedings of the Microwave Symposium Digest, 1998 IEEE MTT-S International. Baltimore, MD, USA, 1998, volume 2, pp. 1055–1058.

[41] Encoder Measurements: How-To Guide. [WWW]. National Instruments, March 2012. Available from: http://www.ni.com/white-paper/7109/en [cited 13 September 2012].

[42] Borenstein, J., Feng, L. Measurement and Correction of Systematic Odometry Errors in Mobile Robots. IEEE Transactions on Robotics and Automation, 12, 6, (1996), December, pp. 869–880.

[43] Carlson, C., Gerdes, J., Powell, J. Error Sources When Land Vehicle Dead Reckoning with Differential Wheelspeeds. The Journal of The Institute of Navigation, 51, 1, (2004), pp. 13–28.

[44] Taylor, G., Brunsdon, C., Li, J., Olden, A., Steup, D., Winter, M. GPS Accuracy Estimation Using Map Matching Techniques: Applied to Vehicle Positioning and Odometer Calibration. Computers, Environment and Urban Systems, 30, 6, (2006), November, pp. 757–772. Available from: http://www.sciencedirect.com/science/article/pii/S0198971506000159 [cited 16 November 2012].

[45] Pegasem GSS Series Microwave Ground Speed Sensors. [datasheet]. Pegasem Messtechnik. Available from: http://www.pegasem.com/english/datasheets_uk/GSS15_25_uk.pdf [cited 21 September 2012].

[46] SCC1300-D02 Combined Gyroscope and 3-Axis Accelerometer with Digital SPI Interfaces. [datasheet]. VTI Technologies. Available from: http://www.vti.fi/sites/default/files/documents/scc1300_d02_datasheet-extensive-v1.0.4.pdf [cited 29 December 2011].

[47] SCC1300-D02 Combined Gyroscope and 3-Axis Accelerometer with Digital SPI Interfaces. [datasheet]. Murata Electronics. Available from: http://www.muratamems.fi/sites/default/files/documents/scc1300-d02_datasheet_v2.1.pdf [cited 23 November 2012].

[48] NI-845x Hardware and Software Manual. [manual]. National Instruments Corporation, June 2011. Available from: http://www.ni.com/pdf/manuals/371746c.pdf [cited 9 February 2012].

[49] Rotary Measuring Technology, Incremental Shaft Encoder, Standard Type Series 5802. [datasheet]. Kübler Group, January 2006. Available from: http://www.kuebler.com/PDFs/archiv/drehgeber/5802_en.pdf [cited 2 January 2012].

[50] Linear Measuring Technology, Measuring Wheels. [datasheet]. Kübler Group, October 2010. Available from: http://www.kuebler.com/PDFs/leaflet/drehgeber/english/Messrad_en.pdf [cited 21 February 2012].

[51] Linear Measuring Technology, Spring Encoder Arm. [datasheet]. Kübler Group, October 2010. Available from: http://www.kuebler.com/PDFs/leaflet/drehgeber/english/Drehgeber_Federarm_en.pdf [cited 20 February 2012].

[52] USB4 Encoder Data Acquisition USB Device. [datasheet]. US Digital. Available from: http://www.usdigital.com/assets/general/239_usb4_datasheet_0.pdf [cited 24 February 2012].

[53] USB4 Encoder Data Acquisition USB Device User Manual. [manual]. US Digital, May 2009. Available from: http://www.usdigital.com/assets/general/USB4%20Manual_0.pdf [cited 24 February 2012].

[54] LM2940/LM2940C 1A Low Dropout Regulator. [datasheet]. National Semiconductor Corporation, July 2005. Available from: http://www.farnell.com/datasheets/7427.pdf [cited 5 March 2012].

[55] LD1117xx Adjustable and Fixed Low Drop Positive Voltage Regulator. [datasheet]. STMicroelectronics, February 2012. Available from: http://www.st.com/internet/com/TECHNICAL_RESOURCES/TECHNICAL_LITERATURE/DATASHEET/CD00000544.pdf [cited 7 March 2012].

[56] GetTickCount Function. [WWW]. Microsoft, March 2012. Available from: http://msdn.microsoft.com/en-us/library/windows/desktop/ms724408(v=vs.85).aspx [cited 25 March 2012].

[57] Motor Driven Rotary Tables, B5990TS Motorized Rotary Table. [WWW]. Velmex. Available from: http://www.velmex.com/motor_rotary_tables.html#6 [cited 26 August 2013].

[58] Keymeulen, D., Peay, C., Yee, K., Li, D. Effect of Temperature on MEMS Vibratory Rate Gyroscope. Proceedings of the IEEE Aerospace Conference, 2005. Big Sky, MT, USA, 2005, pp. 1–6.